Helsinki University of Technology

Department of Electrical and Communications Engineering

Laboratory of Electronics Production Technology

ESPOO 2006 TKK-EPT-15

COMBINED THERMAL, THERMODYNAMIC AND KINETIC MODELLING FOR THE RELIABILITY OF HIGH–DENSITY LEAD-FREE SOLDER INTERCONNECTIONS

Hao Yu

Dissertation for the degree of Doctor of Science in Technology to be presented with due permission of the Department of Electrical and Communications Engineering, Helsinki University of Technology, for public examination and debate in Auditorium S4 at Helsinki University of Technology (Espoo, Finland) on the 15th of November, 2006, at 12 noon.

Helsinki University of Technology
Department of Electrical and Communications Engineering
Laboratory of Electronics Production Technology

Teknillinen Korkeakoulu
Sähkö- ja tietoliikennetekniikan osasto
Elektroniikan valmistustekniikan

Electronics Production Technology Publication Series

TKK-EPT-15

SUPERVISOR

Professor Jorma Kivilahti, D.Sc. (Tech)
Department of Electrical and Communications Engineering
Laboratory of Electronics Production Technology
Helsinki University of Technology

REVIEWERS

Kejun Zeng
Dr. of Technology, MGTS
Semiconductor Packaging Development
Texas Instruments, Inc., USA

Senior Technology Manager Mikko Talvitie, D.Sc.
Nokia Oyj, Itämerenkatu, Helsinki

OPPONENT

Professor Heikki Jalkanen, D.Sc.(Tech.)
Helsinki University of Technology
Materials Science and Engineering
Laboratory of Metallurgy

Senior Technology Manager Mikko Talvitie, D.Sc.
Nokia Oyj, Itämerenkatu, Helsinki

Distribution:
Helsinki University of Technology
Department of Electrical and Communications Engineering
Laboratory of Electronics Production Technology
P.O. Box 3000
FIN-02015 HUT
Finland
Tel: +358 9 451 4991
Fax: +358 9 451 5776
E-mail: Hao.Yu@hut.fi

ISBN 978-951-22-8463-4 (printed)
951-22-8463-4
ISBN 978-951-22-8464-1 (PDF)
951-22-8464-2
ISSN 1457-0440

Espoo 2006
Otamedia Oy

Abstract

Continuous miniaturization of electronics devices as well as increasing complexity of soldering metallurgy introduce more and more challenges to the reliability of modern electronics products. Although loading condition plays an important role, the reliability of solder interconnections is ultimately controlled by microstructures' responses to loading. It is therefore of great importance to understand and control the microstructural evolutions of solder interconnections under different loading conditions. Since experimental investigation alone is inadequate for achieving such knowledge, the employment of different modeling tools is of great help. In this thesis, combined usage of thermal, thermodynamic and kinetic modelling was introduced and utilized in studying solidification and interfacial reactions in solder interconnections.

In order to study the solidification of interconnections during reflow soldering, an oven-level thermal model was first constructed to simulate the flow field inside a typical reflow oven. With the oven information collected, the thermal models were established to simulate the solidification of lead-free solder interconnections. Thermodynamic calculations, which were integrated into the model, provided the thermal properties of the solder alloy used in the experiments. Further, thermodynamic calculations were combined with the nucleation kinetic analyses to evaluate the actual solidification temperatures of interconnections.

The combined thermodynamic and kinetic approach was used also for studying the interfacial reactions between solder and component or board metallizations. For having better understanding of the effect of Ni in solder interconnections, the Sn-Cu-Ni system was assessed thermodynamically. Firstly, the effect of Cu-content on the formation of the primary interfacial intermetallic compounds between near-eutectic SnAgCu solder alloys and Ni-substrate was evaluated as a function of temperature. Secondly, it was analyzed how the Ni dissolved in Cu_6Sn_5 compound affects the driving forces for the diffusion fluxes and hence the growth kinetics of $(Cu,Ni)_6Sn_5$ and $(Cu,Ni)_3Sn$ reaction layers between near-eutectic SnAgCu solder and Cu(Ni) metallizations. With the preliminary kinetic considerations, the shrinkage of $(Cu,Ni)_3Sn$ as well as other related observations in the reaction zone were investigated. Finally, the interfacial reactions of near-eutectic Sn–Ag–Cu solder with Ni(P)/Au metal finishes were studied theoretically and experimentally.

Preface

The researches of this thesis have been carried out in the laboratory of Electronics Production Technology of the Helsinki University of Technology. I am most grateful to my supervisor Professor Jorma Kivilahti, not only for introducing me into the wonderful world of electronics production, but also for his guidance in regard to theoretical and practical aspects of the thesis. His enthusiasm and persistency in scientific knowledge has constantly encouraged and inspired me, which was one of the preconditions to finalize this thesis.

I want to thank all the colleagues in the laboratory of Electronics Production Technology, especially the co-authors Vesa Vuorinnen, Dr. Tomi Laurila, Dr. Toni Mattila. The extensive discussions with them have been an abundant source of ideas. Special appreciation goes to Dragos Burlacu, who works as an active colleague as well as a friend making the office life more colourful. I am also grateful to Pia Holmberg for her patience in the bureaucracy of arranging timely all my documents. Among all the appreciations, I am thankful for all the colleagues, especially Pia Holmberg and Pirjo Kontio, for their assistance in my Finnish life and answering sometimes my "peculiar" questions.

I deeply appreciate my experience in the Phase Diagram Center (PDC) of the Central South University in China. The leader of PDC, Academician Prof. Jin Zhanpeng, gave me not only the basic knowledge of thermodynamics and kinetics but also the courage in exploring unknown world. The memory of PDC is cherished also because of the opportunity of getting acquaintance with so many good friends. Dr. Kejun Zeng and Weiqun Peng are surly among them and should receive the most earnest thanks for their kind help and encouragement.

Especially I dedicate this thesis to my parents and sisters for the continuous support I received in my life. As the youngest spoiled son and brother, I owe them too much and there is nothing I can do to pay back. The same appreciation goes to my mother-in-law who gave me another family full of affection and love.

Finally, and above all of these, I want to express my sincere gratitude to my wife, Juan, for her endless love and support. No words will ever be enough to express my thanks and love for her, and I would like to present this thesis as a part of the celebration of our 7th anniversary of marriage.

Espoo, July 2006

Hao Yu

Table of contents

List of Publications

Publication I H.Yu and J.K.Kivilahti, "CFD modelling of the flow field inside reflow oven", *Journal of Soldering & Surface Mount Technology*, **14**, 1, (2002), pp. 38-44.

Publication II H.Yu, T.T.Mattila and J.K.Kivilahti, "Thermal simulation of the solidification of lead-free solder interconnections", *IEEE Transaction on Component and Packaging Technologies*, **29**, 3, (2006), pp. 475-485.

Publication III H.Yu and J.K.Kivilahti, "Nucleation kinetics and solidification temperature of SnAgCu interconnections during reflow process", *IEEE Transaction on Component and Packaging Technologies* (in print).

Publication IV H.Yu, V.Vuorinen and J.K.Kivilahti, "Solder/substrate interfacial reactions in Sn-Cu-Ni interconnection system", *Journal of Electronic Materials* (in print).

Publication V H.Yu, V.Vuorinen and J.K.Kivilahti, "Effect of Ni on the formation of Cu_6Sn_5 and Cu_3Sn intermetallics", presented in *the 56th Electronic Components and Packaging Technology (ECTC)*, San Diego, CA, May 30–June 2, 2006, pp. 1204-1209; *IEEE Transactions on Electronics Packaging Manufacturing* (in print).

Publication VI V.Vuorinen, T. Laurila, H.Yu, and J.K.Kivilahti, "Phase formation between lead-free SnAgCu solder and Ni(P)/Au finish on PWB", *Journal of Applied Physics*, **99**, 2, (2006), pp. 3530-3536.

Author's Contribution

The researches have been planned and carried out by the author together with the co-author J.K.Kivilahti. The author has been responsible for writing the publications I-V. He performed all the theoretical simulations in these Publications, including thermal models, thermodynamic assessments/calculations, and kinetic analyses. The concept of combining different modeling tools was developed through extensive discussions with the co-authors, while the details of data exchange among them were figured out completely by the author. Temperature measurement of reflow soldering in Publication I and II were carried out by the author and the experimental observations of interconnection microstructure came from the co-authors' researches (T.Mattila and V.Vuorinen).

In Publication VI, the author contributed to develop the idea on the mechanism of interfacial reactions and did the thermodynamic calculations.

Notions

a	activity
A	area of catalytic surface
c_p	specific heat
c	number of components
C	concentration
D	diffusion coefficient (or diffusivity)
D^*	tracer diffusion coefficient
D_{int}	integrated diffusion coefficient
$\tilde{D}$	interdiffusion coefficient
$\tilde{D}_0$	frequency factor for diffusion coefficient
e	internal energy
F	degree of freedom in phase rule
$f(\theta)$	$=\frac{1}{4}(2+\cos\theta)(1-\cos\theta)^2$
$\mathbf{g}$	vector of gravity.
G	Gibbs free energy
h	Plank's constant, 6.625×10^{-34}J/s
H	enthalpy
I_{heter}	nucleation rate
I^0_{heter}	pre-exponential coefficient of nucleation rate
J	diffusion flux, intrinsic diffusion flux
$\tilde{J}$	interdiffusion fluxes
k	thermal conductivity
k_B	Boltzmann's constant, 1.381×10^{-23}J/K
k^r_{B1}, k^d_{B1}	rate constants of reaction-control and diffusion-control regimes
k_x, k_y,, k_z	thermal conductivities in x, y, z directions
$\bar{k}$	kinetic energy of turbulence
M	mobility
N	number of atoms involved in nucleation
N_0	Avogadro's Number, 6.022×10^{23}
N_A	atomic fraction of component A
p	pressure

P	number of co-existing phases
$\dot{q}$	heat-generating rate
q	heat flux
Q	heat produced per unit mass.
Q_d	activation energy for diffusion coefficient
R	universal gas constant, 8.3145 J/mol•K
r^*	critical size of nucleation
S	entropy
t	time
T	temperature.
T_s, T_∞	surface and surrounding temperatures
U	internal energy
v	relative velocity between the Kirkendall and Matano frames
$\mathbf{V}$	vector of fluid velocity
V	volume
V_m	molar volume
v_x, v_y,v_z	components of fluid velocity in x, y, z directions
X	atomic percentage
Δg	free energy change per unit volume of nucleus formation
ΔG^*	nucleartion energy (barrier)
∇	vector differential operator. ∇^2 ($=\nabla\bullet\nabla$) is the Laplacian operator.
α	the convective heat transfer coefficient
$\dot{\varepsilon}$	turbulence dissipation rate
ε	emissivity of solid surface
θ	contact angle
υ	coefficient of viscosity
μ	chemical potential
$^\circ\mu$	standard chemical potential of pure element
ρ	density
σ	interfacial tension

1. Introduction

Since the appearance of calculator in 1960s, highly integrated portable electronic devices have been continuously changing our life. People are now enjoying the conveniences brought by notebook computer, mobile phone, digital camcorder, personal digital assistants (PDAs), and many other personal facilities. The reliability of these products is not only an interest of the electronics industry but also a public concern. Among all the practical challenges, the reliability of solder interconnection appears to be increasingly important for the two following reasons.

With the constant miniaturization of small-scale, high-density electronic products, the volume of solder interconnection has been remarkably reduced during the past decades. Interconnections in the fine pitch components nowadays are only of several hundreds of microns in diameter and contain only several colonies of grains. The reliability of such small interconnections is extremely sensitive to dissolution from substrate, intermetallic formation, and phase transformation. These effects have to be well understood and completely controlled during manufacture. The challenges would be even more critical in the future, when solder volume possibly decreases into the range of 10^{-4} –10^{-5} mm^3. As an example, the thickness of intermetallic layers is believed to be the limit of reducing interconnection size [1].

The effort of eliminating lead-containing materials also causes lots of reliability concerns. According to EU legislation [2-4], the use of lead in electronic products will be restricted to below 0.1 wt% after July 2006, except for high melting temperature solders. The replacements for conventional tin-lead solders have to be found for manufacturers. Among the various candidates [5-7], SnAgCu is the most widely adopted [8-12]. In general, lead-free solders are Sn-based alloys, which have significantly different metallurgical properties from the conventional tin-lead solder. The elevated melting temperature (217°C for SnAgCu, for example) indicates not only difficulties in controlling reflow temperature but also accelerated intermediate compound formation, which increases the risk of interfacial failures.

The reliability of interconnections is a combined result of the physical properties of solder and the loadings applied, but ultimately decided by the microstructure of interconnections [13]. The most important microstructural units in interconnections are the cells, dendrites, colonies of Sn together with second-phase

particles like Cu_6Sn_5 and Ag_3Sn. The amount, shape, and distribution of second-phase particles are particularly important from the viewpoint of plastic deformation, recovery, and recrystallization. Intermediate compounds layer (IMC) also has critical influences on the behaviour of interconnections. Since all these microstructural units are formed through the solidification during reflow process and develop with time, better understanding of the microstructural evolution of interconnection is necessary.

Many researches have been carried out to study the microstructure of interconnection up to now. Different techniques, including optical microscope, X-ray, electronic microscope, have been applied effectively for this purpose. However, due to the complexity of soldering metallurgy, the mechanism of microstructural evolution of interconnection could not be revealed merely by experimental observations and frequently diverse and contradict results are obtained by different researchers.

Models from different physic backgrounds provide effective tools when they are cooperated with each other. As an example, Fig.1 illustrates all the physical and chemical changes occurred in an interconnection during reflow soldering, in which it is heated up to 240-250°C and subjected to a cooling of 1-2°C. The melting and solidification of solder are determined by the thermodynamic properties of solder but

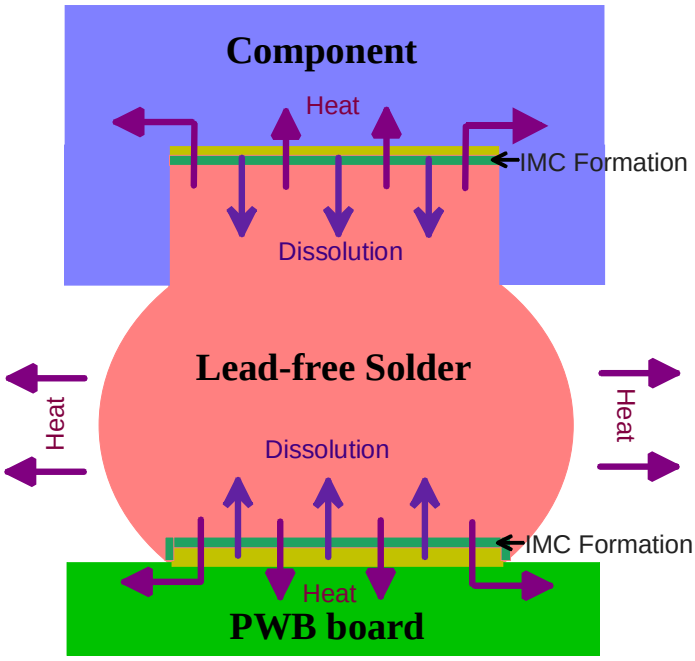

Fig.1 Physical and chemical changes of solder interconnection during reflow process

also influenced by many other factors: 1) Once solder is melted and contacts printed wiring boards (PWB) coating or under bump metallizations (UBM) of component, dissolutions of the elements in the solid surfaces occur and intermetallic compounds form at the interfaces; 2) The required supercooling of liquid solder could be significant, depending on nucleation kinetics; 3) The latent heat of solidification has to be dissipated effectively. These thermal, thermodynamic and kinetic issues are highly correlated with other.

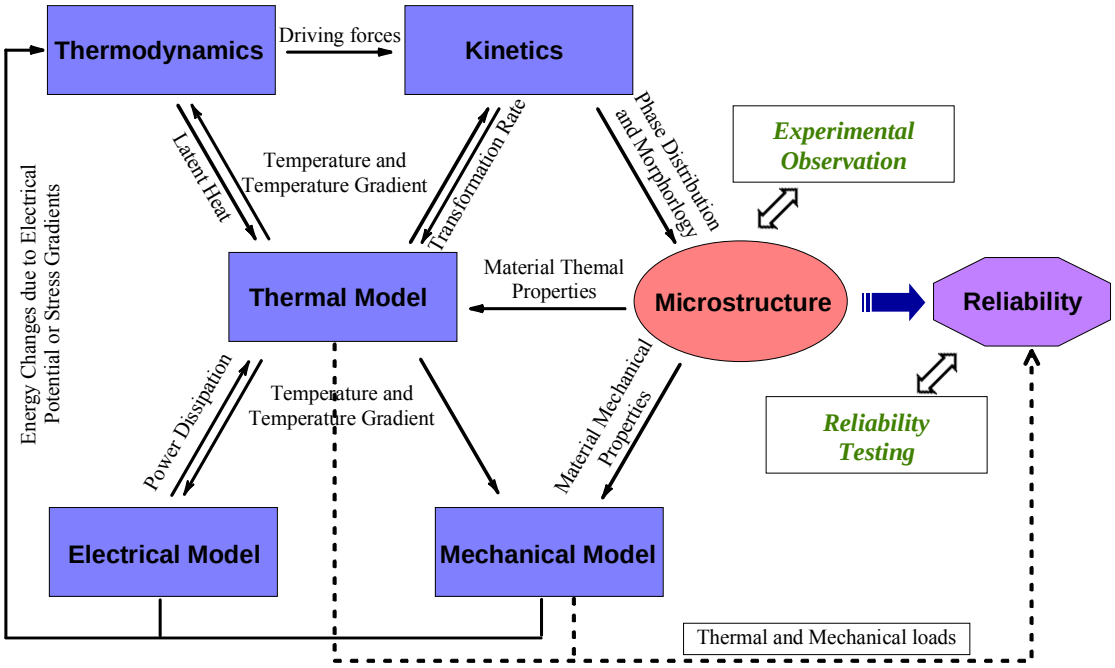

Fig.2 The relationship between theoretical modelling tools and their roles in the study of interconnection reliability.

Fig.2 illustrates the relations between different modelling tools and how they are expected to cooperate with each other. Thermodynamic modelling provides the necessary data, for instances, driving force for kinetic analysis and latent heat for thermal simulations; kinetic models determine how phase transformations start and proceed, which are important issues in thermal simulations; Thermal modelling focuses on temperature fields and offers the key parameters, temperature and temperature gradient, for both thermodynamic and kinetic models. By combining these theoretical tools, the microstructural evolution of interconnections can be studied effectively.

The combined usage of all the theoretical modelling tools shown in Fig.2 is recognized as a promising method of studying the reliability of interconnection. This includes the employments of mechanical and electrical simulations as well. However, such tasks are very demanding and require more extensive efforts from various physical backgrounds. As a major part of the approach presented in Fig.2, the cooperation among thermal, thermodynamic and kinetic simulations are considered in this thesis.

In the following context, Chapter 2 provides a brief discussion on how the reliability of interconnection is related to microstructure. Details on thermal, thermodynamic and kinetic modelling are then described in Chapters 3-5 respectively. A brief summary of the findings in the studies, which contributed to the six publications, is finally given in Chapter 6.

2. Microstructure and Reliability

The reliability of interconnection means the probability that it provides both electrical connection and mechanical support under stated conditions over stated periods of time. The failure mechanism of interconnection can be various, depending on both loading and interconnection microstructure. In this chapter, the relationship between reliability and microstructure is reviewed under various loading conditions.

2.1 Thermomechanical Loading

Electronic products contain many active components that generate heat and raise the temperature of assembly. Since printed wiring boards are composed of various materials with different coefficients of thermal expansion (CTE), the change of temperature introduces dissimilar thermal deformations among different parts. For instance, the CTE of the typical substrate material, FR-4, is around 16×10^{-6}/°C [14], being considerably larger than the CTE of silicon, 2.5×10^{-6}/°C [15]. The mismatch of their thermal expansions results in the deformation of solder interconnections and the variation of thermomechanical stress with temperature causes low cycle-strain-controlled fatigue fail of interconnection [16].

Thermal cycling test is designed to study the reliability of interconnection under temperature variations. It is also referred as thermal shock test when the

ramping rate of temperature is relatively fast as shown in Fig.3. The failure mechanism under thermal shock loading has been widely studied by many researchers [17-22]. It was observed that cracks always take place inside the matrix of solder along or close to intermetallic layers. The propagation of cracks, and therefore the reliability of interconnection, relies on the properties of solder matrix.

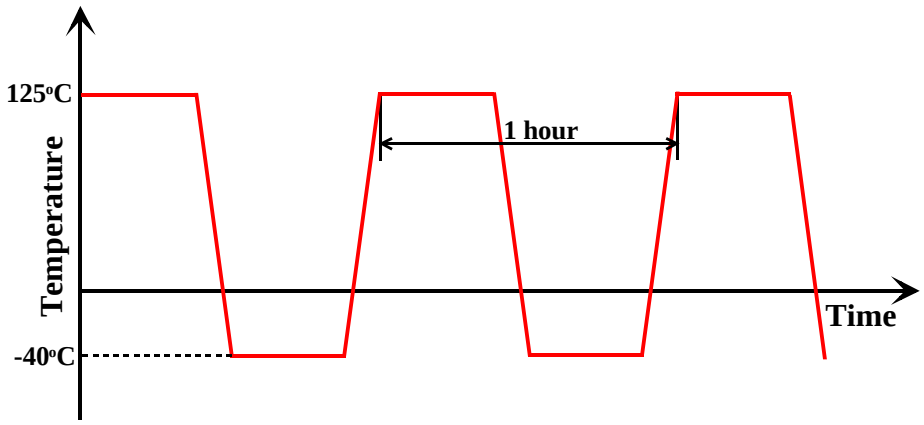

Fig.3 Typical temperature profile of thermal shock test.

Fig.4 depicts the microstructural evolution and the corresponding failure mechanism of Sn-Ag-Cu solder interconnections during thermal shock test [22]. The as-solidified interconnection contains only a few large colonies separated by high angle boundaries [23]. Inside each colony, small Cu_6Sn_5 and Ag_3Sn are dispersed between Sn cells. The high-angle boundaries between colonies are rarely parallel to the most favoured direction of crack propagation so that cracking has to go through the colonies. This is, however, difficult because the Sn cells are almost uniformly oriented inside each colony.

The plastic deformation during thermal shock test provides a driving force for recrystallization from such microstructures. The most likely places for recrystallization are those severely deformed areas like the corners of interconnection. Recrystallized structure is composed of many small grains with random orientations and the boundaries among them provide a good possibility for cracks to nucleate and extend. It is therefore the expansion of recrystallizated areas that eases intergranular fracture of interconnections. Such a mechanism can be clearly seen in Fig.4 with the help of polarized optical micrographs.

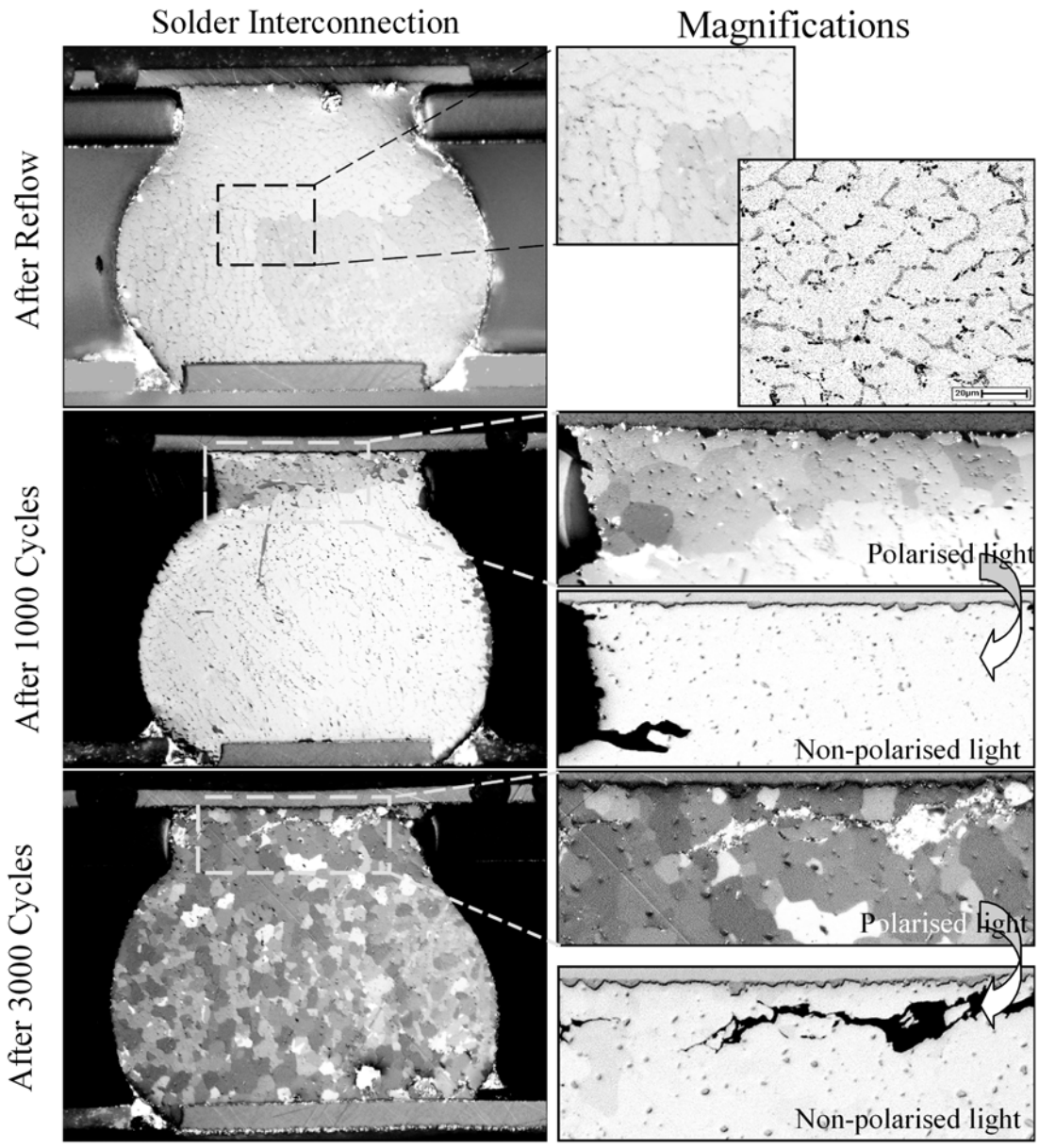

Fig.4 Microstructural evolution and failure mechanism of solder interconnections of a CSP component in thermal shock test [22].

Another method of investigating the reliability under thermomechanical loading is power cycling test. Instead of environmental temperature change, it uses the internal power of active components to heat test boards. It offers a better understanding on the reliability of interconnections in real life. Usually no enhanced cooling can be applied so that temperature varies only between room temperature (25°C) and maximum temperature (around 125°C). It was reported that there is no difference in the failure mechanisms between power cycling and thermal shock tests [24], simply because the loadings are of the same thermal-mechanical type.

Some researches have been carried out to compare the solder joint reliabilities during power cycling and thermal cycling tests, in terms of the same extreme temperatures (25-125°C) [25-27]. The results of these studies indicated that the reliability in power cycling is better than the reliability in thermal cycling. This is because the temperature field is very much localized in power cycling and components are always hotter than board, reducing the difference of thermal expansion and thus the thermal-mechanical stress level.

Another comparison with different extreme temperatures [24], however, reported that the test boards under the power cycling (30-125°C) failed faster than the boards under the thermal shock test (-40-125°C) despite of the higher thermo-mechanical stresses in the thermal cycling. The reason is that the interconnections are kept at a much higher overall average temperature during the power cycling test, which accelerates the recrystallization procedure and helps the cracks to propagate through the interconnection. These results emphasized the importance of understanding the failure mechanism and microstructural evolution in reliability tests.

2.2 Mechanical Shock Loading

Even though the thermomechanical performance of electronic devices is critical, portable products are more vulnerable to the mechanical shock when they are dropped accidentally. The component boards bend and vibrate excessively due to the forces transmitted through product case [28-30]. The displacement between board and components causes the concentration of mechanical stresses and results in component, solder interconnection, or board failures. Board-level drop test is therefore often introduced in order to study the reliability under such situations [31-32].

Since the melting temperature (T_{mp}) of lead-free solder is mostly between 217-227°C (490-500K), interconnections are always working at high homologous temperatures, that is, the temperatures above $0.5T_{mp}$ (around -25°C) in Kelvin [33]. The strength of solder is therefore strain-rate dependent. As examples, the measured flow stresses of three SnAgCu solder alloys are plotted in Fig.5 [34]. Since the strain rate in drop test (≈300 %/s) is much higher than that in thermal cycling ($\approx 3\times10^{-4}$ %/s), solder behaves as a relatively strong material in drop test, which alters the stress distributions inside interconnection. According to simulations, the maximum stress in

drop test is about two times larger than that in thermal cycling and the stresses are more likely to concentrate in the corner of interconnection.

Intermetallic layers are therefore relatively weak and crack goes through the intermediate layers of interconnection as shown in Fig.6. For this reason, interfacial structure plays a critical role in the reliability of interconnection. Depending on the

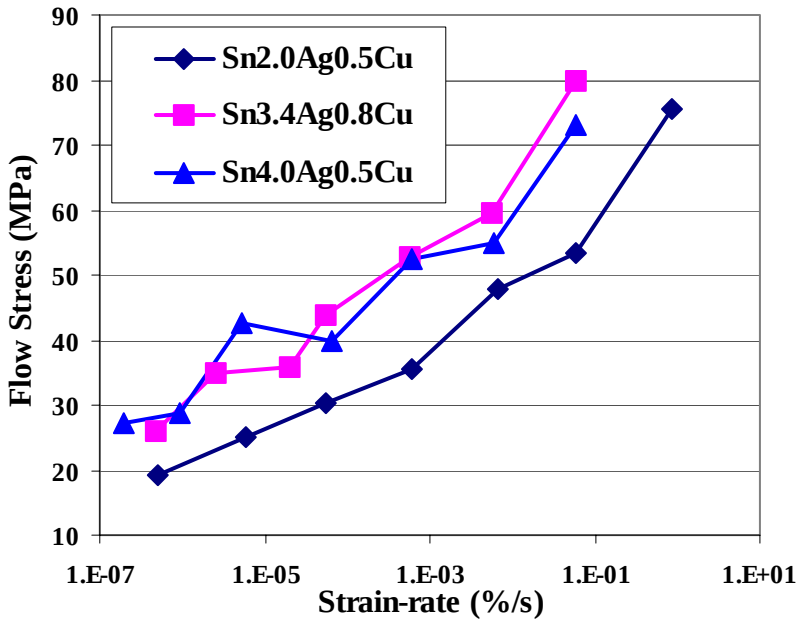

Fig.5 Measured flow stresses versus strain rate of three SnAgCu solder alloys of different compositions [34].

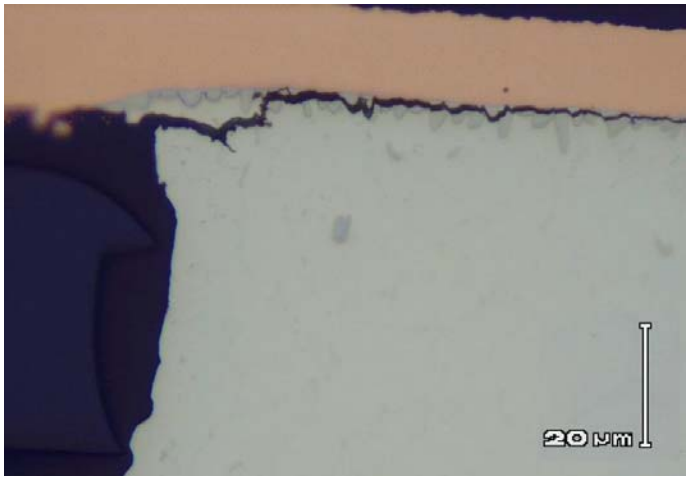

Fig.6 Cracking through the intermetallic $(Cu,Ni)_6Sn_5$ layer of an interconnection in drop test. [33].

solder as well as the metallization used on board/component, different failure mechanisms may be observed. When the same electrochemical Ni is applied on the component side, for instance, PWB coatings was reported to be the most important factor influencing drop testing reliability [33,35]. Organic solderability preservative (OSP) coating appeared to be superior to Ni(P)|Au coating under such a situation, simply as the result of different interfacial microstructure and failure mechanism.

Because OSP coating evaporates quickly during reflow soldering [22], the dissolution of Cu pad into liquid solder is considerably large when it is used as PWB coating. On the board side, Cu_6Sn_5 and Cu_3Sn form sequentially as the typical interfacial structure between Sn-based solder and Cu substrate [36]. On the component side, $(Cu,Ni)_6Sn_5$ is observed instead of Ni_3Sn_4 due to the existence of Cu in the solder [37-40]. Since the mechanical properties of Cu_6Sn_5 is weakened by the Ni dissolved [41], the failure of interconnection occurs more often on the component side, with severe cracking in the brittle $(Cu,Ni)_6Sn_5$ layer [33, 35].

When Ni(P)|Au coating is applied on board, however, $(Cu,Ni)_6Sn_5$ forms on the both sides of the interconnection. Because Ni is always deposited together with a

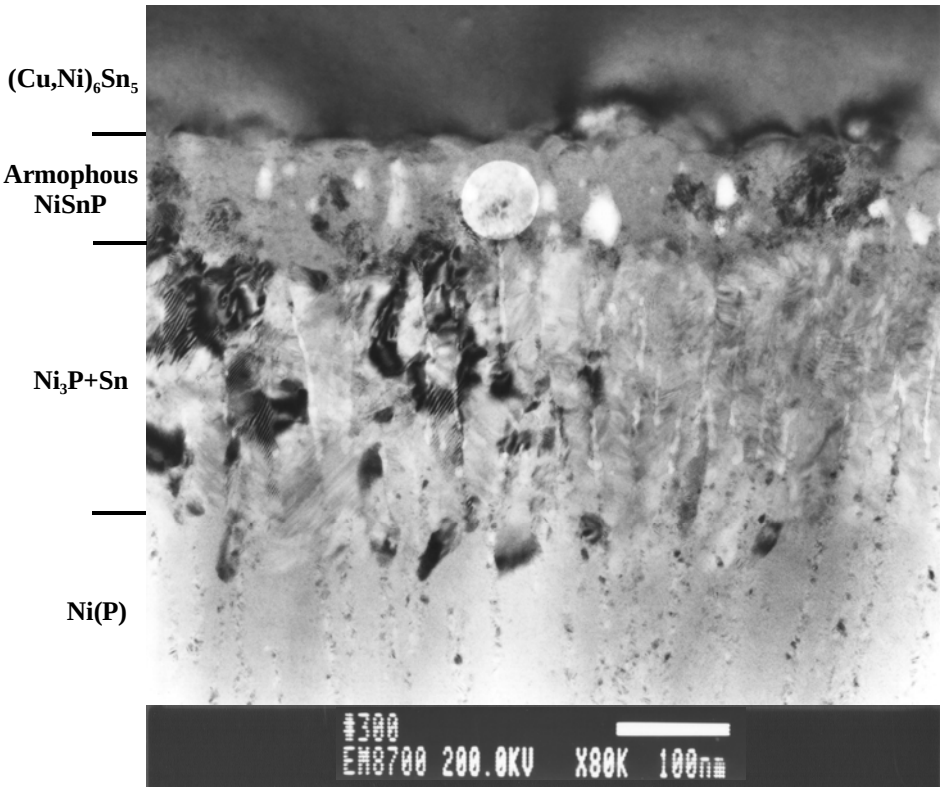

Fig.7 Bright-field image of the reaction zone between electroless Ni(P) and near-eutectic SnAgCu solder, revealing a thin, porous layer of amorphous NiSnP.

large amount of phosphorous (up to 15wt%) during electroless coating, two additional thin layers of high phosphorous-content exist between the Ni(P) coating and the $(Cu,Ni)_6Sn_5$ layer on the board side. As shown in Fig.7, the layer next to the coating is composed of columnar Ni_3P and pure Sn. There is another porous, amorphous (or microcrstalline) NiSnP layer on the top of it. The detailed mechanism of the formation of these layers was investigated in Publication VI and some other explanations were also given in the literatures [42-43]. It is the porous amorphous layer that provides a favourable path for crack propagation and makes interconnection exceptionally weak in drop test. This problem is often known as the "black pad" problem associated with electroless Ni(P)|Au PWB coating.

In a recent study, the components on as-soldered test boards were heated to 75°C and 100°C by integrated thermal elements during drop test. The reliability was found to be better than the drop test reliability at room temperature [44]. It is interesting that cracks go at least partly through the bulk solder, which is similar as the failure mechanism in thermal cycling. Although the reason for such a difference in failure mechanism is not very clear, the different characteristics of microstruture evolution at high temperature is probably responsible for it.

2.3 Consecutive Multiple Loadings

Since portable devices are often dropped after working for a period of time, usually interconnections are subjected to consecutive thermomechanical and mechanical loadings. In a recent study, thermal cycling or isothermal annealing was carried out before drop test [45]. It was found that cracking is no longer restricted in intermetallic layers and different failure mechanisms can be observed depending on the history of test boards.

The thermal cycling before drop test can introduce two different changes to the microstructure of interconnections: 1) The thermal mechanical strain and elevated temperature induces recrystallization in highly deformed region and fatigue cracks along large angle grain boundaries are developed; 2) The thickness of intermetallic layers increases and the interfacial structure evolves with time. The first change weakens the mechanical properties of bulk solder in the following drop test so that the cracking occurs partly through bulk solder [45].

Without temperature variation, the isothermal annealing has only the aging effects to interfacial microstructure. Since the effective time for intermetallic growth is approximately only the total time of the upper soak stages in thermal cycling [46], intermetallic layers have much more time to grow during isothermal annealing. If copper UBM is used on the component side, the formations of Cu_6Sn_5 and Cu_3Sn follow the typical growth kinetics [47-51]. Given adequate time, the formation of "Kirkendall void" in the Cu_3Sn layer [52-53] is much more severe during isothermal annealing and the rupture of intermetallic layer becomes the primary failure mechanism, which degrades the reliability in the following drop test significantly [45].

As a summary of Chapter 2, it has been revealed that the fracture of interconnection may occur in many different ways under diverse situations. The characteristic of loading play an important role, but ultimately the reliability is decided by how microstructure responds to the loading. In order to achieve better understanding on the microstructural evolution of solder interconnection, combined usage of theoretical tools is necessary and becomes the main target of this thesis.

3. Thermal Modelling

Temperature is a critical parameter involved in the both sides of reliability problem: the loading condition and the material behaviour. It affects not only the thermomechanical loading applied to solder interconnections, but also the microstructural evolution under loading. Experimental measurement is the most direct way in revealing temperature fields, but its usage is subjected to practical limitations, especially when the detailed temperature distribution in the vicinity of interconnection is desired. That is why thermal modelling is often utilized in reliability studies. It is frequently cooperated with structural analysis to determine loading conditions, but seldom used in investigating the microstructural evolutions of interconnection, which is also important in obtaining fundamental understandings of reliability. Hence, this chapter focus only on the thermal modelling for studying microstructural evolutions.

There are two stages of microstructural evolution in solder interconnection: the formation of as-solidified structure and its changes later. The thermal models applied in both stages are considered separately in this chapter.

3.1 Thermal Model of Reflow Process

As an essential part of modern surface mount technology, reflow soldering is a delicate technique requiring comprehensive considerations on melting, wetting, solidification, interfacial reactions, and other issues. Many soldering defects can be correlated with improper temperature profile either directly or indirectly [54]. Most importantly from reliability point of view, the as-solidified microstructure acts as the starting point of the microstructural evolution of interconnection. Hence, the temperature profile of reflow process needs to be investigated in great details.

Although thermocouple and data logger are widely employed in recording reflow profiles, some limitations should be notified. Both the size and thermal mass of thermocouples could be comparable with or even larger than small components and the temperature distribution may be disturbed so much that accurate results are inaccessible. The usage of alternative temperature measuring techniques, such as infrared camera or integrated thermal resistors in chip, is also restricted by the nature of reflow process (limited space, high temperature and the movement of boards). For these reasons, computational simulation is of great interest for its capability of visualizing the temperature field around interconnections.

Several researchers [55-63] have contributed to reflow modelling since early 1990's. A thermal approach has been first suggested by Sarvar and Conway [55] and developed by their colleagues [56-59]. It presented simplified models aiming at on-line predictions of reflow profile but the extension to interconnection level is difficult. Another approach proposed by Eftchious et al [60,61] combined an oven model and a card model. Despite of the 2D simplification, it was proved to be successful and adopted also by other researchers later [62,63]. However, due to the fact that IR (infrared radiation) reflowing was still widely used in the 1990's, these works focused only on radiation and natural convection. Since the electronic industry has moved to forced convection reflowing [64], comprehensive model for heating gas is now desired and new approaches have to be introduced.

The ultimate objective of reflow modelling is very demanding and can be only achieved with hierarchical steps. Models of different levels are necessary: large-scale model or oven model, and small-scale model or board model. The reason is that oven information can only be collected in large-scale model, while detailed temperature distributions have to be revealed with small-scale models.

3.1.1 Large-Scale Model

Usually reflow oven consists of several heating zones and one cooling zone, in which interconnections are heated to around 25°C above the liquidus temperature of solder and then subjected to a cooling of 1°C/s–2°C/s. The efficiency of heat transfers between oven and boards relies on the flow field of heating/cooling fluid inside oven. Computational fluid dynamics (CFD) [65-68] simulations could be helpful in collecting such information. The principle of CFD technology is numerically solving a set of flow equations (Navier-Stokes equations) based on the universal conservation laws of mass, momentum and energy. For incompressible Newtonian fluid with constant density, the equations take relative simple forms as follows,

Mass conservation:

$$\nabla \cdot \mathbf{V} = 0 \tag{3-1}$$

Momentum conservation:

$$\rho \frac{D\mathbf{V}}{Dt} = \rho \mathbf{g} - \nabla p + \upsilon \nabla^2 \mathbf{V} \tag{3-2}$$

Energy conservation

$$\rho \frac{De}{Dt} = \frac{\partial Q}{\partial t} + k\nabla^2 T + \upsilon \left[2\left(\frac{\partial v_x}{\partial x}\right)^2 + 2\left(\frac{\partial v_y}{\partial y}\right)^2 + 2\left(\frac{\partial v_z}{\partial z}\right)^2 \right] +$$

$$\mu \left[\left(\frac{\partial v_y}{\partial x} + \frac{\partial v_x}{\partial y}\right)^2 + + \left(\frac{\partial v_z}{\partial y} + \frac{\partial v_y}{\partial z}\right)^2 + + \left(\frac{\partial v_x}{\partial z} + \frac{\partial v_z}{\partial x}\right)^2 - \frac{2}{3}\left(\frac{\partial v_x}{\partial x} + \frac{\partial v_y}{\partial y} + \frac{\partial v_z}{\partial z}\right)^2 \right] = 0 \tag{3-3}$$

In these equations, ∇ is the vector differential operator and ∇^2 (=$\nabla \bullet \nabla$) is the Laplacian operator. t is time, ρ is the fluid density and p is the pressure. $\mathbf{V}$ is an vector of fluid velocity and its three components v_x, v_y,v_z are in the x, y, z directions respectively. $\mathbf{g}$ is the vector of gravity. e is the internal energy and Q is the heat produced per unit mass. T is temperature. υ and k are the coefficient of viscosity and thermal conductivity.

Since turbulent vorticity develops easily near the nozzles of heating/cooling gas, suitable turbulence model also needs to be applied. In one of the most frequently used two-equation $\bar{k}-\dot{\varepsilon}$ model, two additional equations of the variables $\bar{k}$ (kinetic energy of turbulence) and $\dot{\varepsilon}$ (turbulence dissipation rate) are introduced.

With suitable geometric model established, the above equations can be solved numerically and the distributions of those variables, such as temperature, pressure, and velocity, are obtained. This offers a good basis on the evaluation of convective heat transfer coefficients on board/component surfaces.

Another challenge for the oven level CFD model of reflow process might be the movement of boards, which can be only simulated by complex transient model. Fortunately the moving speed of boards is slow compared with the high speed of heating/cooling gas so that simulation on the steady state flow field inside the oven, as presented in Publication I, offers a good approximation.

3.1.2 Small-Scale Model

Small-scale models zoom into the vicinity of boards or components. Conduction becomes much more important and convection plays only the role of surface effect. In such cases the convective heat flux q can be approximated by a simplified equation:

$$q = \alpha\left(T_\infty - T_s\right) \tag{3-4}$$

where α is the convective heat transfer coefficient, T_s and T_∞ are the surface and surrounding temperatures.

The control equation of conduction is

$$\frac{\partial}{\partial x}\left(k_x \frac{\partial T}{\partial x}\right) + \frac{\partial}{\partial y}\left(k_y \frac{\partial T}{\partial y}\right) + \frac{\partial}{\partial z}\left(k_z \frac{\partial T}{\partial z}\right) + \dot{q} = \rho c_p \frac{\partial T}{\partial t} \tag{3-5}$$

Here, $\frac{\partial T}{\partial x}$, $\frac{\partial T}{\partial y}$, and $\frac{\partial T}{\partial z}$ are temperature gradients, k_x, k_y, and k_z are thermal conductivities in different direction, $\dot{q}$ is the heat-generating rate, ρ and c_p are the density and specific heat of material, $\frac{\partial T}{\partial t}$ is the time dependency of temperature. By using finite element method (FEM), Equation (3-5) can be solved numerically.

Depending on the domain of interest, small-scale models can be also created hierarchically at board, component, and interconnection levels. High-level models provide the boundary conditions of low-level models and the temperature distribution of interconnections can be revealed gradually by this means. As an example, Fig.8 shows the results from a component model and an interconnection model. In the

interconnection model, it is to be noticed that the effect of phase transformation of solder becomes significant and thermodynamic approaches has to be integrated as described in Publication II.

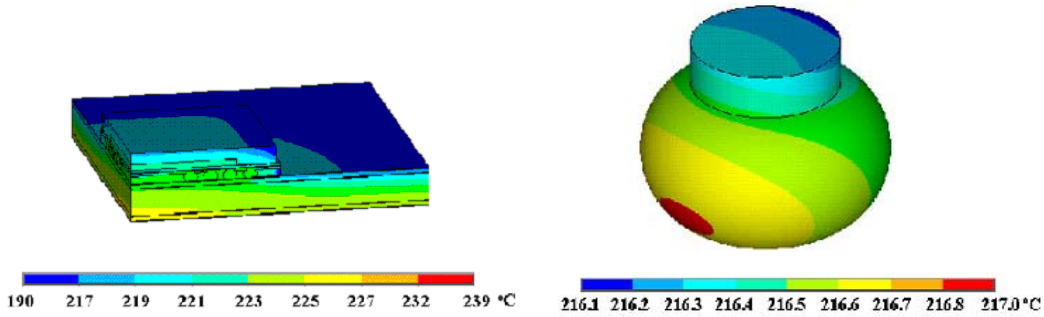

(a) (b)

Fig.8 Results from small-scale solid models during the cooling of a reflow process. (a) component model; (b) interconnection model.

3.2 Thermal Model in Service Stage

During the service of electronic devices, temperature and temperature distribution around interconnection is critical for understanding its microstructural evolution. Thermal modelling is therefore also an effective tool at this stage. Depending on the objective and accuracy required, simulations of different levels can be employed similarly.

In order to reduce cost, natural convection is preferred in the thermal design of electronic devices but forced convection is also often used. Either CFD simulation can be performed or average convective heat transfer coefficient can be used in evaluating convective heat fluxes.

Due to the low thermal conductivity of printed wiring boards, temperature field around components is usually localized. The maximum temperature could be considerably high compared with the surrounding temperature but restricted only within small regions. Hence, the role of radiation becomes considerably important. Normally radiative heat flux is presented as

$$q_{rad} = \varepsilon\sigma\left(T_s^4 - T_\infty^4\right) \tag{3-6}$$

where ε is the emissivity of solid surface, T_s and T_∞ are the surface and surrounding temperatures respectively. For the radiative heat flux between different surfaces, more

complicate approaches need to be introduced to estimate the view factors [69], which depend on both the position and the orientation of the surfaces.

Small-scale models at borad, component, or interconnection level are nearly the same as the ones used in reflow process modelling. The differences are the existence of internal heat sources (in active components, for example) and the oposite direction (from surface to surrounding) of surface heat fluxes. As an example, Fig.9 presents the result of a board level model of a test board with an active component and several passive components.

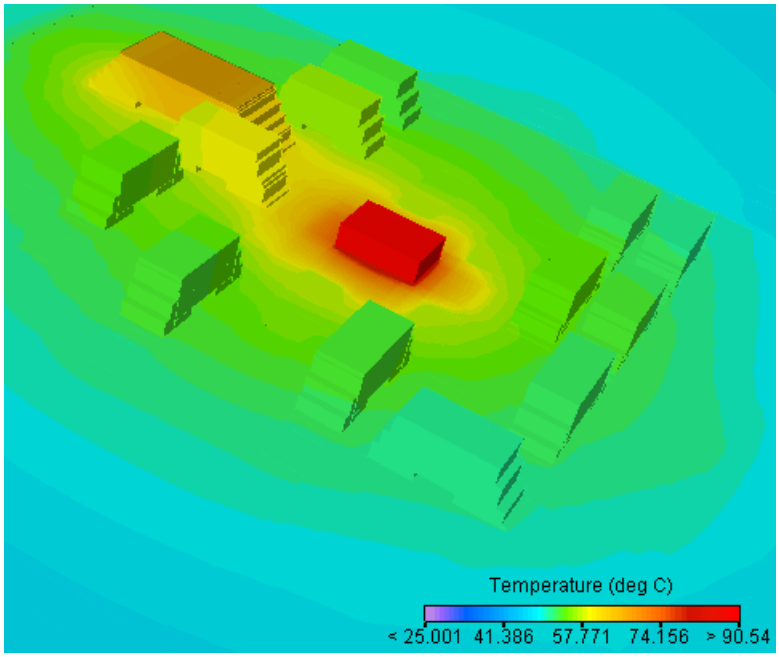

Fig.9 Simulated temperature distribution of a test board on which an active component and several passive components are mounted.

4. Thermodynamic Calculation

Solder interconnection are composed of many dissimilar materials. In order to understand the microstructural formation and evolution, thermodynamic properties of different metallurgical systems have to be known as thoroughly and accurately as possible. Thermodynamic calculation is therefore indispensable and its application in reliability study is described in this chapter.

4.1 Gibbs Free Energy, Chemical Potential and Phase Equilibrium

Based on the combination of the first and second laws of thermodynamics, the characteristic state function for temperature (T) and pressure (p) is the Gibbs free energy, which is defined by the following relation in a closed system:

$$G \equiv U + pV - TS = H - TS \tag{4-1}$$

where U, V, H, and S are the internal energy, volume, enthalpy and entropy of the system. G is additive and the total G of a system is the sum of G of all the phases. Under constant temperature and pressure, the Gibbs free energy of a system tends to decrease spontaneously, that is, an equilibrated system owns the lowest possible Gibbs free energy under specified T and p.

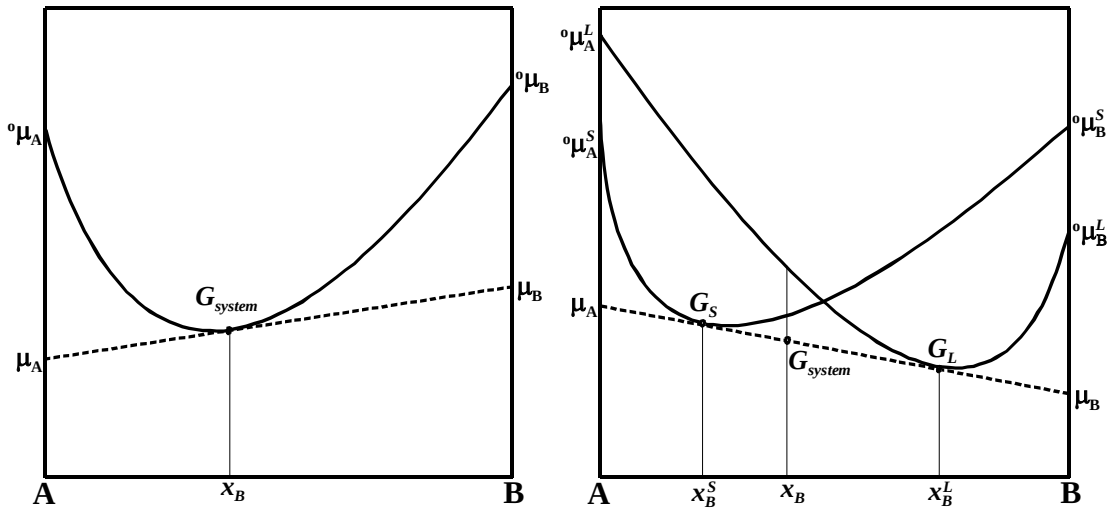

(a) (b)

Fig.10 Gibbs free energy curves and the tangent lines determining chemical potentials in a binary system A-B under constant temperature and pressure. (a) Uniphase system; (b) Two-phase system.

Gibbs free energy is dependent on composition in multicomponent systems. As an example, for the binary system A-B shown in Fig.10 (a), the Gibbs free energy is a function of atomic percentage of B, x_B. If there is only one phase in the system, the Gibbs free energy function is represented by a continuous curve between the elements A and B. Both ends (x_B=0 and x_B=1) of the curve are the Gibbs free energies of pure elements, denoted as $^{\circ}\mu_A$ and $^{\circ}\mu_B$ because they are equivalent with the standard chemical potentials of the elements.

At any composition of x_B, the Gibbs free energy of the system is determined on the curve in Fig 10 (a). If a tangent line to the curve is drawn at the composition, it intersects with the lines x_B=0 and x_B=1 and determines two quantities, μ_A and μ_B. They are the partial Gibbs free energies of A and B at the composition because

$$G_{system} = x_A\mu_A + x_B\mu_B = (1 - x_B)\mu_A + x_B\mu_B \tag{4-2}$$

Although the name and symbol may vary depending on the interest, partial Gibbs free energy is identical to chemical potential. This is why the symbol μ is adopted. Chemical potential measures how much the Gibbs free energy of a system changes if a number of atoms of an element are added while keeping the number of the other atoms (and the temperature T and the pressure p) constant. It is correlated with the activity of element, a, by the following relations:

$$\begin{aligned} \mu_A &= {}^0\mu_A + RT\ln a_A \\ \mu_B &= {}^0\mu_B + RT\ln a_B \end{aligned} \tag{4-3}$$

If there are two phases in a binary system, for instance, solid (S) and liquid (L) phases, two independent Gibbs free energy curves can be plotted as shown in Fig.10(b). They represent the situation when only one of the phases exists and the other phase is always suppressed. The broken line in the figure is the common tangent to the two curves. In the range between the two tangent points (x_B^S and x_B^L), G is minimized only when the two phases coexist and have the compositions x_B^S and x_B^L. Such two phases are in equilibrium with each other. Hence, the traces of x_B^S and x_B^L with the variation of temperature are the boundaries of the corresponding two-phase region in the A-B phase diagram.

Since x_B^S and x_B^L are determined by the common tangent line to the Gibbs energy curves in Fig.10(b), the chemical potentials are the same in both phases, that is, $\mu_A^L = \mu_A^S = \mu_A$ and $\mu_B^L = \mu_B^S = \mu_B$. This agrees with the principle that the chemical potential of all elements should be uniform in an equilibrated system. The phase equilibria in ternary or higher order systems are determined in the same manner, but with larger number of independent variables in the Gibbs energy functions.

4.2 The Phase Rule and Phase Diagram

The phase rule determines the degree of freedom *f* of equilibrium state, which is the number of independent variables that may vary without changing the equilibrium, that is, without changing the existence of any phase. It is expressed as

$$f = c - p + 2 \tag{4-4}$$

where *c* is the number of components and *p* the number of co-existing phases. The number 2 on the right side comes from the two external variables, temperature and pressure. For metallic system, in most cases pressure can be regarded as constant so that the phase rule reduces to

$$f = c - p + 1 \tag{4-5}$$

Phase diagram is a common type of state diagram carrying the information of phase equilibrium. Normally it is presented in the temperature-composition space under constant pressure. The space is divided into numbers of domains, inside which certain phase equilibria are expected. Depending on the number of phases, there are domains for single-phase, two-phase, three-phase and so on. The domains may appear as point, line, area, or volume in the space, depending on the degree of freedom *f*.

When the pressure is fixed in metallic systems, binary phase diagrams are two-dimensional with composition being *x*-axis and temperature being *y*-axis. Three-dimensional construction is required for ternary phase diagrams and commonly equilateral triangle is applied to present compositions. Due to the inconvenience of plotting three-dimensional drawings, practically isothermal or vertical sections of ternary phase diagrams are utilised. It becomes even more difficult to schematically present higher order phase diagrams and some variables has to be fixed before any two-dimensional diagram can be obtained.

As an example, Fig.11 shows the binary Sn-Cu phase diagram [70]. Except the liquid, solid Cu and Sn, there are also several intermetallic phases in the system, including the important compounds in soldering metallurgy, Cu_6Sn_5 (η) and Cu_3Sn (ε).

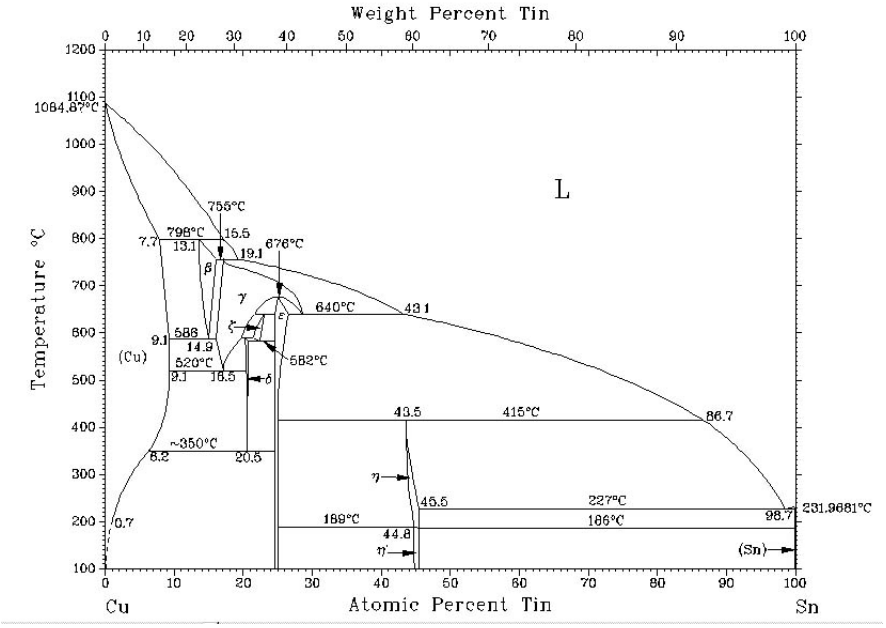

Fig.11 Sn-Cu binary phase diagram [72].

4.3 Thermodynamic Assessment

Since phase diagram is a manifestation of equilibrium states, it can be easily constructed once the thermodynamic properties of a system are known. In order to achieve such an objective, analytical expressions of the Gibbs free energies of phases are required and they can be derived by means of thermodynamic assessment. The most successful approach of thermodynamic assessment is known as the CALculation of PHAse Diagrams (CALPHAD) method [71,72].

In the CALPHAD technique, thermodynamic models are first introduced to evaluate the Gibbs free energy of different phases. In most cases, unknown parameters are inevitable so that they are only semi-empirical models with fundamental physical assumptions. The unknown variables are obtained through optimisations aiming at the best fit to all the experimental information, including both phase equilibria and thermochemical data. Once this procedure is finished, a description of the system is established and further calculations are enabled.

Depending on the structural characteristics and composition range of different phases, different models can be applied. The most common models are the substitutional solution model and the sublattice model. The substitutional solution model assumes that all the elements are almost randomly mixed so it is relatively

simple and suitable for liquid or other solution phases. The sublattice model assumes there are several independent sublattices with fixed mole fractions and it is suitable for those phases with superlattical structure like intermetallic compounds. More details concerning the models can be found in literature [73].

4.4 Thermodynamic Calculations

Thermodynamic description of solder interconnection system offers a good opportunity to obtain fundamental information in studying many metallurgical procedures, such as solidification and interfacial reactions. They provide quantitative evaluations of both phase equilibrium and thermodynamic data. Information on metastable equilibria, which are usually not achievable experimentally, can be also obtained by suppressing some phases. These are beneficial for the studies on the microstructural formation and evolution of solder interconnections [74].

4.4.1 Evaluation of Phase Equilibrium

Thermodynamic assessment is first of all a powerful tool in evaluating critical phase equilibrium information, when experimental determination is difficult or the results are controversial. A good example is in the development of eutectic Sn-Ag-Cu solder. Although the eutectic temperature at 217°C has long been well determined, the reported eutectic compositions scatter in a large area [75-77]. Thermodynamic calculation in the Sn-Ag-Cu system was therefore applied and helped to determine the eutectic composition (Sn-3.38Ag-0.84Cu) [78]. Another example is the investigation of three phase equilibrium of liquid(Sn) + $(Cu,Ni)_6Sn_5$ + $(Cu,Ni)_3Sn_4$. Due to the small solubilities of Ni and Cu in liquid Sn, experimental determination of the liquid composition is difficult and thermodynamic evaluation appeared to be effective (see Publication IV).

Frequently metastable equilibrium information is of great importance, especially in understanding the mechanisms of soldering reactions. However, seldom can they be obtained experimentally and thermodynamic calculation is the only way to estimate them. For example, immediately when liquid Sn contacts any solid surface, the elements in solid dissolve into the liquid. Before intermetallic compounds form at the interface, dissolutions of the elements are limited by their metastable solubilities in liquid Sn determined by the metastable liquid/solid equilibrium. With

the Gibbs free energies of liquid and solid phases, extrapolations to metastable regions provide reasonable estimations of the metastable solubilities.

With the increase of the number of elements involved in lead-free soldering metallurgy, another advantage of thermodynamic calculation is the capability of predicting phase equilibria in high-order system. In fact, thermodynamic description of a multi-component system always starts from its sub-systems, such as binary, ternary, quaternary systems and so on. When there is little information available in high-order system, direct extrapolation from sub-systems has been proved to be helpful in limiting the experimental effort of determining the relations of phase equilibrium.

4.4.2 Representation of Phase Transformation

Since phase diagram carries the information of phase equilibria under specific conditions, it tells also how phase transformations should occur with the change of any state variable, for instance, the solidification of solder alloy during cooling. Depending on cooling rate and the nature of the system, solidification can be investigated with two different assumptions: 1) phase equilibrium is achieved fully in the system; 2) phase equilibrium is only achieved locally inside the system. The thermodynamic calculations under both assumptions require the descriptions of the system with the CALPHAD technique applied.

If solidification happens slowly in such a manner that the system can be regarded as being completely in equilibrium all the time, it is referred as "equilibrium solidification" and its thermodynamic calculation is straightforward. As an example, Fig.12(a) is the calculated liquids projection of the Sn-Ag-Cu phase diagram, which is obtained by projecting the liquidu surfaces into the composition triangle. Fig.12(b) is the vertical section of the phase diagram along the line A-A' (x_{Cu}=0.01). Considering a solder with the composition x_{Cu}=0.01 and x_{Ag}=0.01 (Sn0.91Ag0.54Cu, marked as point *a* in the figures), solidification starts with the formation of primary Sn at the temperature of T_1 (226.0°C). When the temperature drops to T_2 (222.4°C), binary eutectic reaction $L \Rightarrow Sn+Cu_6Sn_5$ happens between the primary Sn phases. Finally the solidification ends isothermally at T_3 (216.8°C) with the ternary eutectic reaction $L \Rightarrow Sn+Cu_6Sn_5+Ag_3Sn$. In such a procedure, liquid composition varies along the broken line in Fig.12(a), which is often known as the equilibrium solidification path.

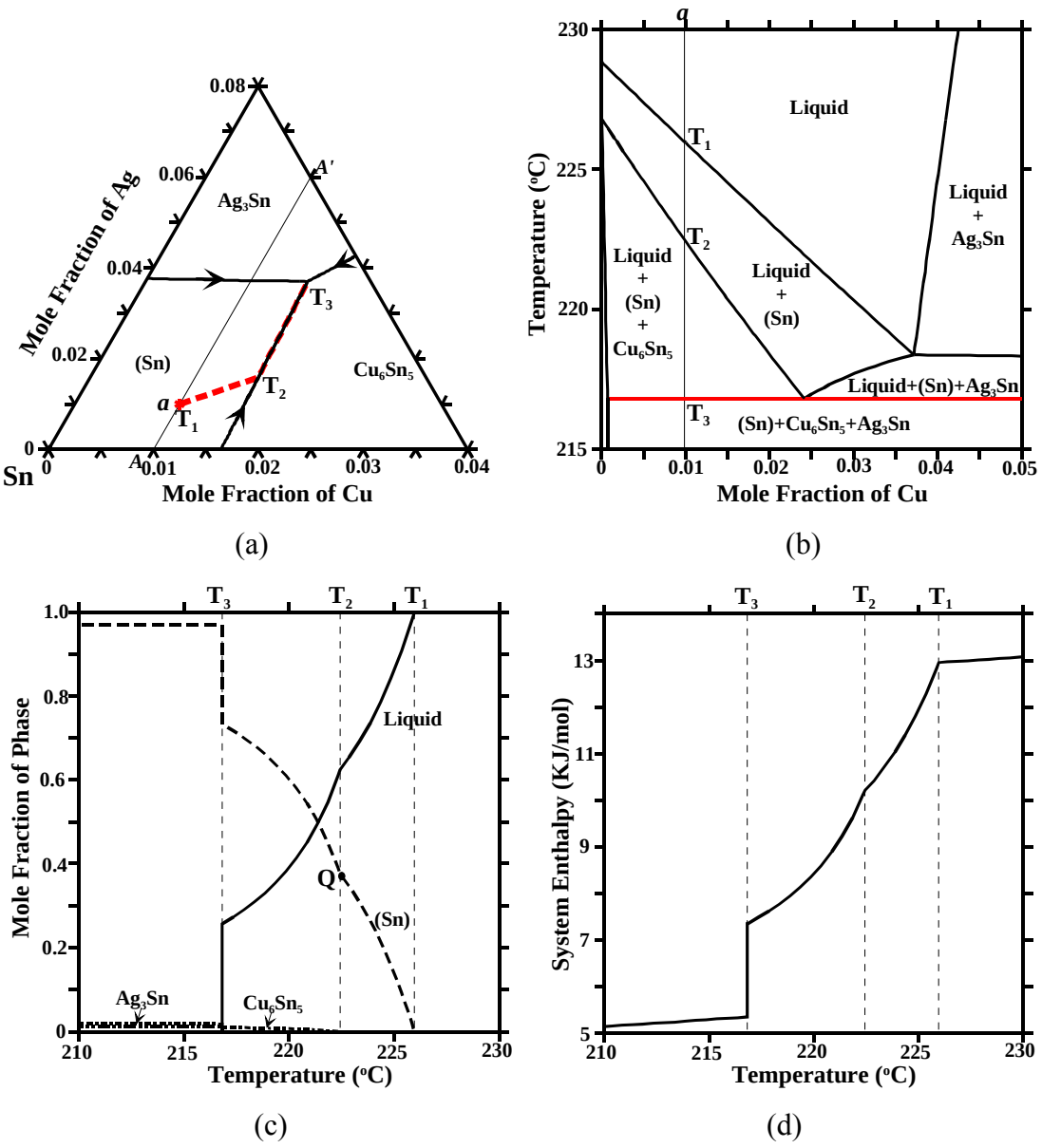

Fig.12 Calculations for the equilibrium solidification of Sn-Ag-Cu solder. (a) Liquidu projection of the Sn-Ag-Cu phase diagram at the Sn-corner; (b) x_{Cu}=0.01 isopleth of the Sn-Ag-Cu phase diagram; (c) NP diagram showing the mole fraction of phases as functions of temperature; (d) System enthalpy as a function of temperature.

Fig.12(c) is the NP diagram showing the variation of the amounts of the phases with temperature. NP diagram is a direct derivation from the calculated ternary phase diagram and useful in studying the evolution of phase transformation. For instance, the amount of primary Sn has been reported to be an important factor affecting the mechanical properties of solder alloy [79] and it can be read at the point Q in Fig.12(c). NP diagrams are also useful for estimating the properties of solder

alloy, including thermal, mechanical, and electrical properties, through averaging the properties of different phases.

The variations of thermodynamic quantities, such as enthalpy and entropy, can be also calculated with the help of NP diagram. Fig.12(d) depicts the variation of the system enthalpy during the solidification procedure stated above. It determines not only the heat capacity of the alloy in specific temperature ranges, but also the thermal effect of isothermal phase transformations.

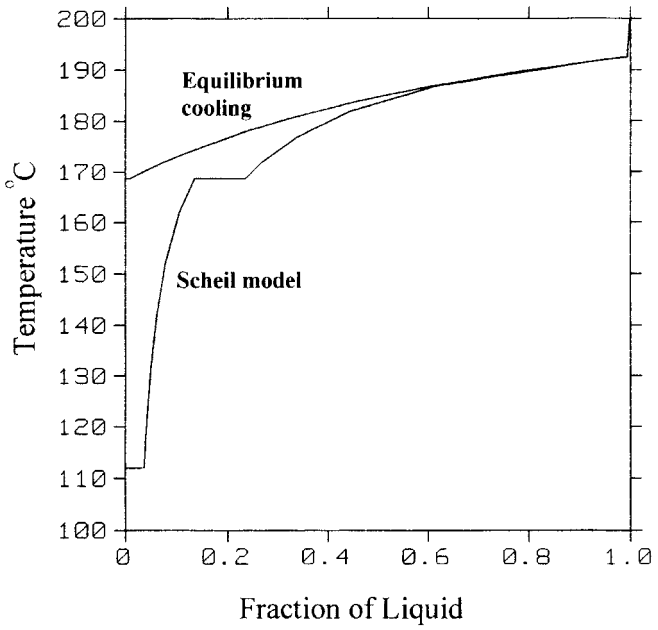

Fig.13 Calculated liquid amounts during the solidification of solder alloy Sn20In3.5Ag based on equilibrium solidification and Scheil model simulations.

In many cases when the cooling rate is high and equilibrium cannot be kept completely in the system, equilibrium solidification fails to describe the actual solidification procedure and local equilibrium assumption becomes helpful. The Scheil model, which assumes that there is a complete mixing in liquid but no diffusion in solid, is frequently applied. This is of great importance for solder alloy, which is subjected to relatively high cooling rate during reflow soldering. For instance, a simulation of the solidification of Sn20In3.5Ag solder has been performed with the Scheil model [80]. As shown in Fig.13, even though the equilibrium solidu temperature of the alloy is 170°C, the simulation revealed that a small amount of liquid remains until the ternary eutectic temperature 113°C, leading to a segregation of the solidified microstructure. Without being homogenized afterwards, this will

result in partial melting at relative low temperature and cause reliability problem of solder interconnection.

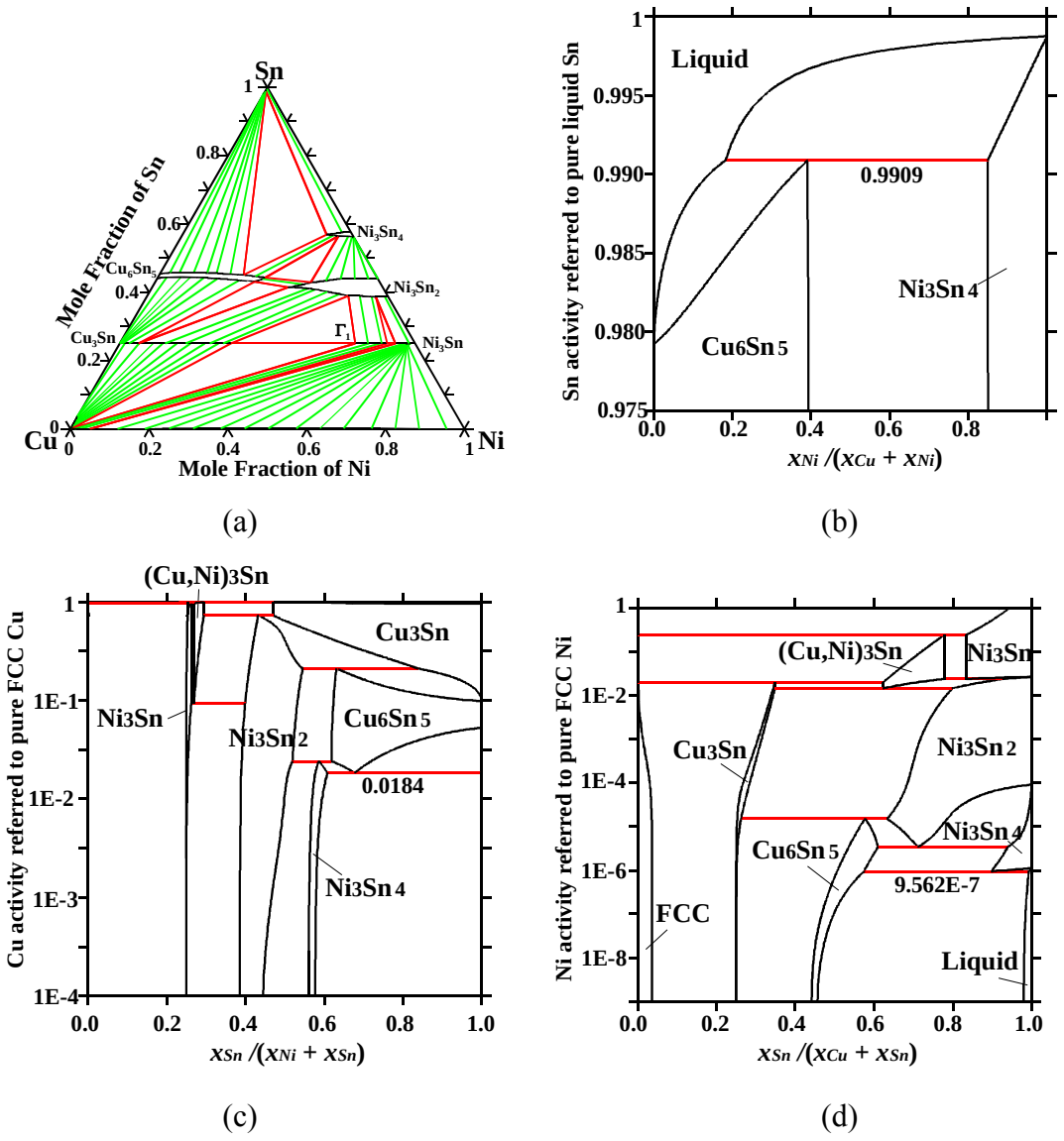

Fig.14 Calculated activity diagrams Sn-Cu-Ni system at 240°C. (a) Isothermal section of the phase diagram; (b) Sn activity diagram; (c) Cu activity diagram; (d) Ni activity diagram.

4.4.3 Calculation for Kinetic Considerations

Although analyses under equilibrium assumption provide fundamental understanding, phase transformation is ultimately controlled by kinetics. However, thermodynamic calculation is also of great importance for its capability of presenting quantitative data for kinetic considerations. For example, driving force is one of the

most important data for kinetic analyses and usually it has to be obtained through thermodynamic calculation.

With local equilibrium and local nominal composition assumed [74, 81], thermodynamic calculation plays a vital role in diffusion kinetics. It is widely used in determine interfacial compositions in a reaction zone. Diffusion path [82,83], which is a set of phase compositions from one end material to the other, can be studied with the help of calculated phase diagrams. They have been proved to be powerful tools in studying solder/substrate interfacial reactions.

Since atoms diffuse always from their high-activity regions to low-activity regions, activity diagram can be applied effectively in studying diffusion kinetics. Activity diagram is a special type of phase diagram and follows the phase rule. It uses the activity of one element as the *y*-axis and the ratio of the other elements as the *x*-axis. Depending on the diffusing element of interest, different activity diagrams need to be established. Once the thermodynamic description of a system is available, however, their constructions are straightforward. For example, Fig.14 shows the isothermal section of Sn-Cu-Ni phase diagram at 240°C together with the activity diagrams for the components Sn, Cu, Ni, respectively.

5. Kinetic Analyses

Although thermodynamics predicts the tendency of microstructural evolutions, it cannot tell how quick a change takes place. Some metallurgical procedures may be suppressed due to kinetic reasons even if they are thermodynamically favoured. In fact, kinetic analyses provides the most direct understandings on the mechanism of microstructural evolution and therefore of great significance in reliability studies.

Advanced kinetic analyses are often restricted from the lack of reliable data. Frequently simplified approaches are necessary from practical point of view and they have to be introduced with cautions. However, this does not limit the importance of quantitative kinetic simulations and they have been approved to be helpful in many cases, especially when they are cooperated with thermodynamic calculations.

5.1 Nucleation Kinetics

Many phase transformations take place through nucleation and nucleation kinetics decides how they start. For instance, the solidification of liquid begins with the nucleation of solid particles. It does not occur immediately when the equilibrium solidification temperature is reached. Certain amount of supercooling, that is, the difference between the actual and equilibrium solidification temperatures, is always required. Usually high-level supercooling is necessary for small-volume liquids so that the supercooling of solder interconnection during reflow soldering could be considerably large [23].

For the sake of convenience, solidification is used to derive nucleation kinetic equations in the following context. The formation of solid phase in liquid is driven by their Gibbs free energy difference as plotted in Fig.15 for a binary system A-B. The temperature of the diagram is slightly lower than the equilibrium solidification temperature so that the solid is stable. Concerning a liquid at the composition x_B^L, the chemical potential of the elements are μ_A^L and μ_B^L respectively. When a small solid nucleus is formed in liquid, its composition is likely to be at x_B^S so that the chemical potentials are lowered as much as possible to μ_A^S and μ_B^S, the change of chemical potentials are then:

$$\begin{aligned} \Delta\mu_A &= \mu_A^S - \mu_A^L \\ \Delta\mu_B &= \mu_B^S - \mu_B^L \end{aligned} \tag{5-1}$$

The free energy change per unit volume associated with the formation of such a nucleus is therefore

$$\Delta g = \left[x_A^S \Delta\mu_A + x_B^S \Delta\mu_B\right] / V_m \tag{5-2}$$

where V_m is the molar volume of the solid. In multicomponent systems, Equation (5-2) becomes

$$\Delta g = \sum x_i^S \Delta\mu_i / V_m \tag{5-3}$$

The formation of the nucleus, however, introduces also an extra interfacial energy that increases the total energy of the system. If the nucleus is sphere, the total energy change is a function of the radius *r*.

$$\Delta G = \frac{4}{3}\pi r^3 \Delta g + 4\pi r^2 \sigma \tag{5-4}$$

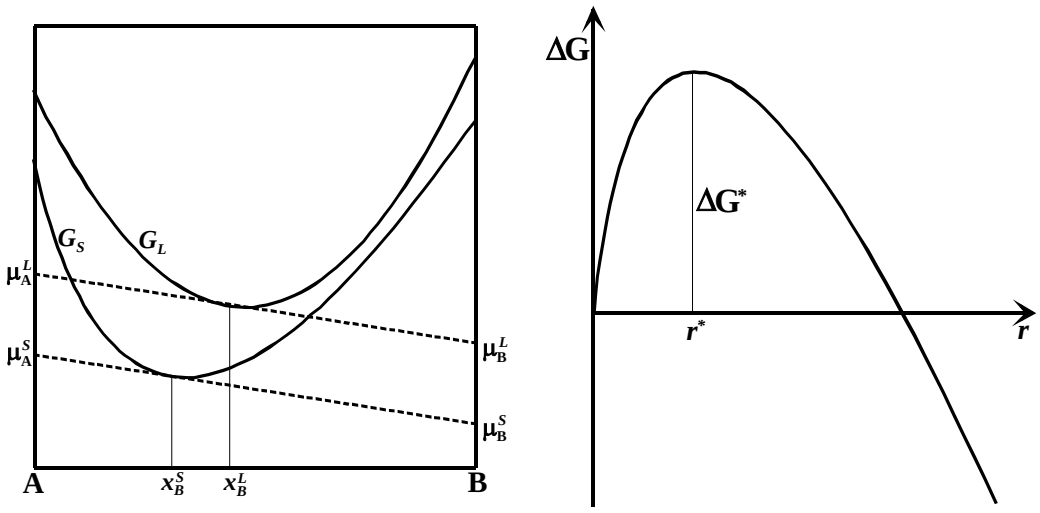

(a) (b)

Fig.15 Energy changes in nucleation. (a) Gibbs free energy-composition diagram of phases; (b) The energy change associated with the formation of a small nucleus, as function of its size. .

with σ being the solid-liquid interfacial tension. The first term on the right side of the equation is negative and proportional to r^3, while the second term is positive and proportional to r^2. As the result, ΔG increases to a maximum first with the increase of r and then decreases as shown in Fig.15(b). The maximum of ΔG is the energy barrier for nucleation ΔG^* and the corresponding r is named as the critical size r^*. Only those nuclei larger than r^* can grow successfully and become effective nuclei. The nucleation energy ΔG^* and the critical size r^* can be derived directly from Equation (5-4):

$$\Delta G^* = \frac{16}{3}\frac{\pi\sigma^3}{\Delta g^2} \tag{5-5}$$

$$r^* = -\frac{2\sigma}{\Delta g} \tag{5-6}$$

Two types of nucleation may occur in supercooled liquid: homogeneous and heterogeneous nucleations. Homogeneous nucleation refers to the nucleation inside liquid. It requires very high-level suppercooling and occurs only in highly purified tiny droplets. Practically heterogeneous nucleation is always the mechanism of initiating solidification. It happens on certain catalytic solid surfaces as shown in Fig.16. Usually solid nuclei are spherical caps on the catalytic surfaces so that the

energy barrier of nucleation is reduced. The shape of the nuclei depends on its contact angle θ on the surface, which determined by the balance of interfacial tensions:

$$\cos\theta = \frac{\sigma_{L,C} - \sigma_{S,C}}{\sigma_{L,S}} \tag{5-7}$$

Here σ denotes the interfacial tensions between different surfaces with *L*, *C*, *S* represent liquid, solid and catalytic phases respectively.

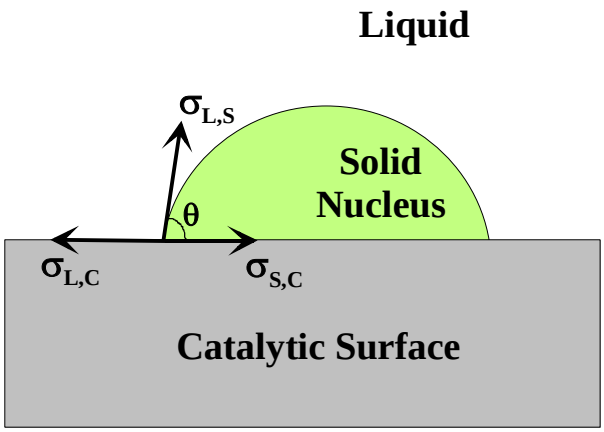

Fig.16 Heterogeneous nucleation on catalytic solid surface in liquid.

According to the classical nucleation theory [84,85], heterogeneous nucleation rate, that is, the number of effective nuclei formed in unit period of time, is expressed by the following exponential kinetic expression:

$$I_{heter} = I_{heter}^{0} \exp\left(-\frac{\Delta G^{*}}{k_B T} f(\theta)\right) \tag{5-8}$$

where k_B is the Boltzmann's constant, I_{heter}^{0} is a pre-exponential coefficient and T is temperature. $f(\theta)$ is a function of the contact angle θ written as

$$f(\theta) = \frac{1}{4}(2+\cos\theta)(1-\cos\theta)^2 \tag{5-9}$$

The coefficient I_{heter}^{0} can be calculated as [85]

$$I_{heter}^{0} = \frac{n k_B T}{h} \exp\left(-\frac{\Delta G_A}{k_B T}\right) \tag{5-10}$$

where h is Plank's constant and n is the number of atoms involved in the nucleation procedure. ΔG_A is the activation free energy for transporting an atom across the

interface, which can be approximated by the activation energy for viscous flow of the liquid.

Only those atoms close to the catalytic solid surfaces are involved in heterogeneous nucleation. Assuming a simple cubic arrangement of the interfacial atoms, n can be presented by

$$n = A \cdot \left(\frac{V_m}{N_0} \right)^{-2/3} \tag{5-11}$$

where V is the molar volume of liquid, A is the total area of the catalytic surfaces, and N_0 is the Avogadro's Number.

With the approach described above, the nucleation rate of solid (β-Sn) in solder interconnection can be calculated as a function of temperature. The nucleation rates are very slow at the temperature close to the equilibrium solidification temperature, but increase abruptly at certain temperatures during cooling. It offers a good opportunity to evaluate the actual solidification temperature of interconnection during reflow soldering (see Publication III).

Nucleation kinetics can be helpful in investigating the formation of intermetallic compounds between liquid solder and solid substrate as well. For example, when Ni exists in lead-free solder interconnection, either $(Cu,Ni)_6Sn_5$ or $(Ni,Cu)_3Sn_4$ can be formed depending on Cu and Ni contents. Although thermodynamic calculations offer a fundamental understanding on which one is preferred under certain situations (see Publication IV), it is their nucleation kinetics that determine the compound to be formed first. This issue is left open due to the insufficient data of both phases.

5.2 Diffusion Kinetics

Diffusion plays an important role in many metallurgical procedures, especially in the growth of interfacial compounds. A lot of practical problems in solder interconnection, such as electromigration and Sn whiskers, are either directly or indirectly correlated with the diffusion of elements. Hence, studies on solid-state diffusion are of practical significance.

Fick's first law describes the diffusion flux of an element in a steady state:

$$J = -D \frac{\partial C}{\partial x} \tag{5-12}$$

where D is called the diffusion coefficient (or diffusivity) in the unit of m^2/s, C is the concentration of the element (mol/m^3) and $\frac{\partial C}{\partial x}$ is its gradient in x-direction. For transient diffusion problem, the continuity equation based on mass conservation is also obeyed and the flux equation of Fick's second law is derived:

$$\frac{\partial C}{\partial t} = D\frac{\partial^2 C}{\partial x^2} \tag{5-13}$$

Since the motions of different atoms are relative to each other, the diffusion fluxes should be determined with a certain frame of reference defined. In a binary system A-B with constant molar volume, the interdiffusion fluxes with respect to laboratory-fixed or Matano frames are the combined result of the two individual diffusion fluxes. Since the sum of the fluxes should be zero, they are presented as:

$$\tilde{J}_A = -\tilde{J}_B = -\tilde{D}\frac{\partial C_A}{\partial x} = \tilde{D}\frac{\partial C_B}{\partial x} \tag{5-14}$$

where $\tilde{D}$ is the interdiffusion coefficient. The interdiffusion coefficient can be regarded as a measure of the mixing rate of the components.

When the Kirkendall frame is used, the fluxes related to mobile lattice site are determined instead and named as intrinsic diffusion fluxes. Because the Kirkendall plane is the original interface prior to diffusion, the intrinsic diffusion fluxes describe the individual movements of the atoms and the sum of them is not zero. There exists a net flux of atoms causing a displacement of lattice planes, which generates the well-known Kirkendall effect. In order to balance the net flux of atoms, vacancies in the lattice should move to the opposite direction in such a manner that,

$$J_A + J_B + J_V = 0 \tag{5-15}$$

The vacancies can be created and annihilated at sources and sinks such as surfaces, internal interfaces or dislocations. However, in some cases vacancies can also condense with each other and form the so-called Kirkendall voids, which lead to reliability problems of solder interconnections [52].

The relationship between the interdiffusion flux and the intrinsic diffusion flux of a component A is given by [86]

$$\tilde{J}_A = J_A + C_A v = J_A - N_A \sum_{i=1}^{n} J_i \tag{5-16}$$

where v is the relative velocity between the Kirkendall and Matano frames and N_A is the atomic fraction of component A. v can be obtained by measuring Kirkendall shifts by using inert markers.

Based on the fact that diffusion is actually driven by chemical potential gradient, a better description of intrinsic diffusion flux is [87],

$$J = -\frac{CD^*}{RT}\frac{\partial \mu}{\partial x} \tag{5-17}$$

D^* is defined as the tracer diffusion coefficient (m^2/s) and R is the universal gas constant (8.3145 J/mol K). If the mobility of diffusing atom is defined as:

$$M = D^*/RT \tag{5-18}$$

it becomes

$$J = -MC\frac{\partial \mu}{\partial x} \tag{5-19}$$

For dilute ideal solution, the relationship between chemical potential gradient and concentration gradient is:

$$\frac{\partial \mu}{\partial x} = \frac{\partial \mu}{\partial C}\frac{\partial C}{\partial x} = \frac{RT}{C}\frac{\partial C}{\partial x} \tag{5-20}$$

The Fick's first law in Equation (5-12) can be then obtained (D=D^*) by substituting Equation (5-20) into Equation (5-17).

For the diffusion fluxes in multi-layer interfacial reaction zones, Equations (5-17) and (5-19) offer a better opportunity of combining kinetic analysis and thermodynamic calculations. They are advantageous for two reasons. 1) The homogeneity ranges of intermetallic compounds is often very narrow, which makes it difficult to use concentration gradient; 2) According to the local-equilibrium assumption, interfacial chemical potentials rely on the equilibrium state between phases. When some phase is newly formed or eliminated from the reaction zone, the chemical potential gradients inside the adjacent layers are altered. When thermodynamic calculation is cooperated, such influences can be taken into account easily in Equations (5-17) and (5-19).

Beside composition, stress and electrical current can also cause chemical potential gradient. Associated with suitable descriptions on such effects, Equation (5-19) can be utilized to study tin-whiskers growth [88], electromigration [89], and other reliability issues related to diffusion.

The interdiffusion coefficient, $\tilde{D}$, can be determined experimentally and often presented as an exponential function of temperature:

$$\tilde{D} = \tilde{D}_0 \exp\left(-Q_d / RT\right) \tag{5-21}$$

$\tilde{D}_0$ and Q_d are named as frequency factor (m^2/s) and activation energy (J/mol). They can be found by using Arrhenius plots of measured $\tilde{D}$. However, it is equally important to notice that diffusion coefficients are dependent on composition. Either Boltzmann-Matano method or Heumann method can be applied to evaluate the average $\tilde{D}$ over concentration ranges. For line compounds, Wagner introduced the integrated diffusion coefficient, D_{int}, as $\tilde{D}$ integrated over the homogeneity range, which is more directly related to experimentally observed thickness of compounds and therefore helpful in investigating the interfacial diffusion kinetics in solder interconnections [50].

5.3 Growth Kinetics of Interfacial Compounds

The growth kinetics of interfacial compounds have received a lot of attentions because IMC layers significantly influence the reliability of interconnection. This has been emphasized recently by the fact that more and more solder/substrate combinations are introduced for lead-free solder interconnections. Due to the complexity of interfacial kinetics, however, it is difficult to cover all the studies and only parts of the fundamental ideas are described in this section.

The growth of intermetallic compounds takes place at the interfaces between different materials when the temperature is high enough for atomic movements. Either the diffusional transport of reaction elements through the product layer or the chemical transformation at the interface can be the controlling factor of the growth kinetics. By taking account of both effects, Dybkov suggested a theory for the solid-state growth kinetics in heterogeneous binary systems [90-92].

Considering a single layer of intermediate compound A_pB_q growing at the interface between pure elements A and B as shown in Fig.17(a), the growth of A_pB_q occurs at the interfaces through the following processes:

Interface (1): $$q\mathrm{B}(\textit{diffusing}) + p\mathrm{A}(\textit{surface}) \Rightarrow \mathrm{A_pB_q} \tag{5-22}$$

Interface (2): $pA(diffusing) + qB(surface) \Rightarrow A_pB_q$ (5-23)

Both processes involve two consecutive steps: (a) diffusion of atoms through the layer A_pB_q; (b) chemical reaction of the diffused atoms with the other atoms at the surfaces. Such processes are usually called the reaction or chemical diffusion.

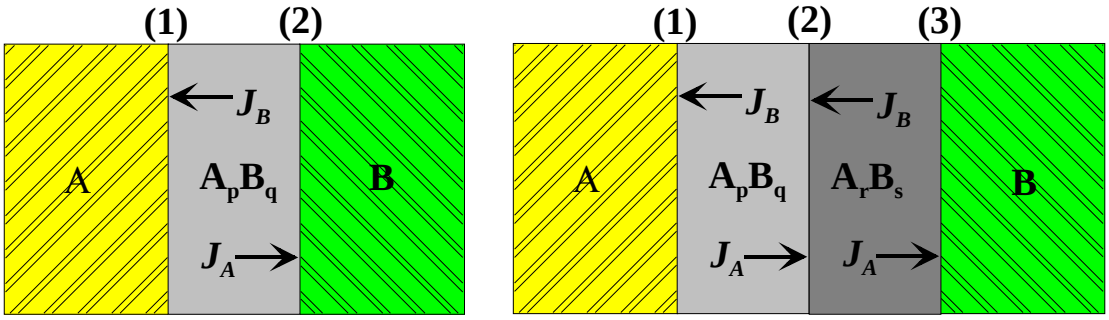

(a) (b)

Fig.17 Growth of intermediate compound layers at the A/B interface. (1) One compound A_pB_q; (b) Two compounds A_pB_q and A_rB_s.

In the initial stage of interfacial reaction, the A_pB_q layer is very thin and the overall rate of reaction is limited by the reactivity at the surface of A or B, which remains constant. The growth rate at the A/A_pB_q interface (marked as interface (1) in the figure) is therefore fixed:

$$\left(\frac{dx}{dt}\right)_{reaction} = k_{B1}^{r} \tag{5-24}$$

where x is the layer thickness and k (m/s) is the rate constant. The superscript of k, r, indicates that it is during the reaction-control regime. In the subscript B1, B shows the atoms that diffuse towards the reaction and 1 shows the interface where the reaction takes place.

When the A_pB_q layer becomes thick enough, all B atoms diffusing from element B react with A atoms instantaneously and the reaction rate is controlled by the B atom flux. During this diffusion-control regime, the growth rate and the rate constant (m^2/s) are:

$$\left(\frac{dx}{dt}\right)_{diffusion} = \frac{k_{B1}^{d}}{x} \tag{5-25}$$

$$k_{B1}^{d} = \frac{D_B\left(C_{B2} - C_{B1}\right)}{C_{B1}} \tag{5-26}$$

If Equation (5-19) is applied to present the diffusion flux, the rate constant can be also obtained with chemical potential difference instead of Equation (5-26):

$$k_{B1}^{d} = M_B\left(\mu_{B2} - \mu_{B1}\right) \tag{5-27}$$

The equations (5-27) and (5-28) represent the growth of A_pB_q layer under two extreme situations. The practical growth rate of A_pB_q at the A/A_pB_q interface can be obtained by summating the reciprocals:

$$\left(\frac{dx}{dt}\right)_1 = \frac{k_{B1}^{r}}{1+\left(k_{B1}^{r}x/k_{B1}^{d}\right)} \tag{5-28}$$

A similar treatment can be applied at the A_pB_q/B interface so that the total growth rate of the A_pB_q layer is:

$$\left(\frac{dx}{dt}\right)_{A_pB_q} = \frac{k_{B1}^{r}}{1+\left(k_{B1}^{r}x/k_{B1}^{d}\right)} + \frac{k_{A2}^{r}}{1+\left(k_{A2}^{r}x/k_{A2}^{d}\right)} \tag{5-29}$$

For small x, where $k_{A2}^{r} << k_{A2}^{d}/x$ and $k_{B1}^{r} << k_{B1}^{d}/x$ can be assumed, the equation (5-32) describes a linear growth of the A_pB_q layer; For large x, where $k_{A2}^{r} >> k_{A2}^{d}/x$ and $k_{B1}^{r} >> k_{B1}^{d}/x$ can be assumed, the equation (5-29) describes a parabolic growth of the A_pB_q layer;

If two compounds, A_pB_q and A_rB_s are growing simultaneously between A and B as shown in Fig.17(b), the same analysis can be applied and the processes involved in the growths of compounds are:

Interface (1): $$q\mathrm{B}(\textit{diffusing}) + p\mathrm{A}(\textit{surface}) \Rightarrow \mathrm{A_pB_q} \tag{5-30}$$

Interface (2): $$(sp-qr)\mathrm{A}(\textit{diffusing}) + r\mathrm{A_rB_s}(\textit{surface}) \Rightarrow s\mathrm{A_pB_q} \tag{5-31}$$

Interface (2): $$(sp-qr)\mathrm{B}(\textit{diffusing}) + r\mathrm{A_pB_q}(\textit{surface}) \Rightarrow p\mathrm{A_rB_s} \tag{5-32}$$

Interface (3): $$r\mathrm{A}(\textit{diffusing}) + s\mathrm{B}(\textit{surface}) \Rightarrow \mathrm{A_rB_s} \tag{5-33}$$

The reactions (5-31) and (5-32) happen at the same interface (2) but on the A_pB_q and A_rB_s side respectively. The difference from single-phase growth here is that the A_pB_q layer is consumed in the process (5-32) and the A_rB_t layer is consumed in the process (5-31). Such influences can be found by using the ratio of the molar volumes of the compounds, $g = V_{A_pB_q}/V_{A_rB_t}$ and the final growth kinetics of the two compounds is presented as:

$$\left(\frac{dx}{dt}\right)_{A_pB_q} = \frac{k_{B1}^{r}}{1+\left(k_{B1}^{r}x/k_{B1}^{d}\right)} + \frac{k_{A2}^{r}}{1+\left(k_{A2}^{r}x/k_{A2}^{d}\right)} - \frac{rg}{p}\frac{k_{B2}^{r}}{1+\left(k_{B2}^{r}y/k_{B2}^{d}\right)} \tag{5-34}$$

$$\left(\frac{dy}{dt}\right)_{A_rB_s} = \frac{k_{B2}^r}{1+\left(k_{B2}^r y/k_{B2}^d\right)} + \frac{k_{A3}^r}{1+\left(k_{A3}^r y/k_{A3}^d\right)} - \frac{q}{sg}\frac{k_{A2}^r}{1+\left(k_{A2}^r x/k_{A2}^d\right)} \qquad (5\text{-}35)$$

where *x, y* are the thickness of A_pB_q and A_rB_s respectively

Depending on the thickness *x* and *y*, different combinations of the rate constants in the equation (5-33) and (5-34) are obtained so that different types of growths are described. For example, if *x*, *y* are small and $k_{B1}^r + k_{A2}^r < \frac{rg}{p}k_{B1}^2$ is satisfied, the A_pB_q layer cannot grow at all. Hence, this approach can be helpful in investigating the growth of IMC layers at solder/substrate interfaces.

6. Summary of the Thesis

This thesis consists of six publications. The primary objective was to achieve better understanding and control of the reliability of solder interconnections by using various modelling tools. The thermal, thermodynamic and kinetic simulations employed in the thesis were proved to be very helpful in investigating the formation and evolution of microstructures in solder interconnections. This is of increasing importance, because microstructural evolution determines failure mechanisms and thus the reliability of electrical interconnections. The thermal modelling was used for finding out the local temperatures of interconnections, while the combined thermodynamic and kinetic modeling were utilised to investigate soldering metallurgies. The three modelling tools were highly cooperated with each other and equally important.

The first part of the thesis, Publications I-III, focused on the formation of as-reflowed microstructure. Based on CFD (Computational Fluid Dynamics) method, an oven-level thermal model was first constructed to simulate the flow field inside a typical reflow oven. It helped to collect the oven information that is needed for establishing the thermal models at component and interconnection levels. With the assumption of complete equilibrium solidification, thermodynamic modeling being integrated into these thermal models provided the thermal properties of solder alloys. The results of the simulations implied that the solder/metallization interfaces on printed wiring board and component side are equally likely sites for initiating the solidification of interconnections. On the basis of the simulated temperature distribution, the growth conditions for the primary Sn crystals during solidification

were also evaluated. Furthermore, thermodynamic calculations were combined with the nucleation kinetic analyses to evaluate the actual solidification temperatures of liquid interconnections. It was revealed that the degree of supercooling (about 18-20°C) of near-eutectic SnAgCu solder interconnections is fairly constant.

In the second part of the thesis, Publications IV-VI, the combined thermodynamic and kinetic approach was used for studying solder/substrate interfacial reactions. In order to understand the effect of Ni in lead-free solder interconnections, the Sn-Cu-Ni system was assessed thermodynamically. With the thermodynamic description of the system obtained, the critical Cu-contents for the $(Cu,Ni)_6Sn_5$ formation between near-eutectic SnAgCu solder alloys and Ni substrate were calculated as a function of temperature. In addition, the influences of Ni on the diffusion fluxes in the reaction zone between Sn-based solder and Cu(Ni)-substrate were investigated. With the kinetic considerations, the shrinkage of $(Cu,Ni)_3Sn$ layer as well as other related experimental observations were investigated. Finally, the evolution of the observed microstructures between the near-eutectic Sn–Ag–Cu solder with Ni(P)/Au metal finishes were also studied based on the mass balance and available thermodynamic data on the Sn–P–Ni system. It was discovered that the metastable nanocrystalline ternary NiSnP layer is the first phase to form and partially transformed into the columnar Ni_3P during cooling.

The main results of each publication are summarized as follows:

Publication I, entitled “CFD modelling of the flow field inside a reflow oven”, outlined a scheme for reflow modelling and presented an oven-level thermal model of the steady state flow field inside a reflow oven, which is needed in subsequent transient analysis and small-scale models as presented in Publication II. The model was constructed by utilising the advanced computational fluid dynamics (CFD) method using commercial software, CFD-ACE+. The computational results were compared with experimentally measured data in the oven.

In publication II, entitled “Thermal simulation of the solidification of lead-free solder interconnections”, two thermal models of different level, a component model and an interconnection model, were established to simulate the solidification of lead-free solder interconnections of a chip-scale packaged component during reflow

soldering. The thermal properties of the interconnections were derived with the help of thermodynamic calculations relevant to the phase transformations occurring during melting and solidification. Experimental measurements were carried out and the data were used to determine some parameters so that the model is more realistic. The results from Publication I was utilised in the determination of heat transfer coefficient during the process. Although the results of the component model agreed with the experimental measurements in the faster cooling of the component than the board, the interconnection model suggested that the temperature gradients over the interconnections were unlikely to be of significance until the invariant eutectic reaction commenced. The findings imply that solder/metallization interfaces on printed wiring board and component sides are equally likely sites for initiating the solidification of interconnections. On the basis of the simulated temperature distribution, the growth conditions of the primary Sn are evaluated and an explanation for the sequence of solidification steps has also been given.

Publication III, entitled "Nucleation kinetics and solidification temperatures of SnAgCu interconnections during reflow process", continued the discussion on the solidification of solder interconnection with combined thermodynamic and kinetic approach focusing on the suppercooling of interconnection. The nucleation kinetics of β-Sn in liquid SnAgCu interconnections was simulated on the basis of nucleation theory. After evaluations of the compositions of liquid solder interconnections during reflow soldering, the free energy of nucleation can be calculated thermodynamically. Since homogeneous nucleation rate is very low, the mechanism that initiates solidification of interconnections is the heterogeneous nucleation at the Liq/Cu_6Sn_5 interface and the corresponding nucleation rates in interconnections are therefore simulated. Additional simulation of the nucleation rate in a tin droplet was also done to determine a critical range of nucleation rate. The contact angle for the heterogeneous nucleation was evaluated with the help of recent DSC measurements. The simulations allow us to evaluate the actual solidification temperature of interconnections, which is a fundamental parameter in studying the formation of solidified microstructure in solder interconnections. The variation of the solidification temperature with cooling rate, interconnection size, and morphology of intermetallic compounds is also discussed. Even though the actual solidification temperatures of

interconnections depend on Ag-content, the supercooling range is shown to be fairly constant (18-20°C), which offers a possibility to predict the actual solidification temperature of interconnections via phase equilibria information.

Publication IV, entitled "Solder/substrate interfacial reactions in Sn-Cu-Ni interconnection system", aims at obtaining better understanding of the effects of interconnection microstructures on the reliability of soldered assemblies. One of the most important ternary systems used in electronics, the Sn-Cu-Ni system, has been assessed thermodynamically. Based on the data obtained, some recent experimental observations related to the formation of interfacial intermetallic compounds in solder interconnections have been studied analytically. Firstly, the effect of Cu-content on the formation of the interfacial intermetallic compounds between SnAgCu solder alloys and Ni-substrate was investigated. The critical Cu-content for $(Cu,Ni)_6Sn_5$ formation was evaluated as a function of temperature. Secondly, it was analyzed how the Ni dissolved in Cu_6Sn_5 compound affects the driving forces for the diffusion of components and hence the growth kinetics of $(Cu,Ni)_6Sn_5$ and $(Cu,Ni)_3Sn$ reaction layers. With the thermodynamic description other experimental observations related to the Sn-Cu-Ni system can be rationalized as well. The system can be utilized also as a subsystem for industrially important higher order solder systems.

Publication V, entitled "Effect of Ni on the formation of Cu_6Sn_5 and Cu_3Sn intermetallics", studied the effect of Ni on the formation of Cu_6Sn_5 and Cu_3Sn intermetallics between tin and (Cu,Ni)-substrates by making use of the thermodynamic assessment of the Sn-Cu-Ni system obtained in Publication IV. The driving forces for the diffusion of the elements in the intermetallic layers were calculated as a function of Ni-content. Assuming constant mobilities of component atoms, the results suggest that the diffusion fluxes of all the components in the $(Cu,Ni)_6Sn_5$ layer increase with increasing content of dissolved Ni, while the Cu and Sn fluxes in the $(Cu,Ni)_3Sn$ layer decrease. Therefore, the dissolution of Ni retards the growth of $(Cu,Ni)_3Sn$. When the Ni-content of the (Cu,Ni) substrate is high enough, the intermetallic compound growth in the reaction zones is dominated by $(Cu,Ni)_6Sn_5$ and the $(Cu,Ni)_3Sn$ layer disappears gradually. The small thickness of $(Cu,Ni)_3Sn$ is associated with large difference between Sn and Cu fluxes in $(Cu,Ni)_3Sn$ that encourages also the "Kirkendall void" formation. In addition, the calculated driving

forces suggest that the growth rate of $(Cu,Ni)_6Sn_5$ should further increase if $(Cu,Ni)_3Sn$ disappears, resulting in an unusually thick $(Cu,Ni)_6Sn_5$ layer. The results of thermodynamic calculations supplemented with diffusion kinetic considerations are in good agreements with recent experimental observations.

In publication VI, entitled “Phase formation between lead-free Sn–Ag–Cu solder and Ni(P)/Au finishes”, the interfacial reactions of near-eutectic Sn–Ag–Cu solder with Ni(P)/Au metal finishes on printed wiring boards as well as in component under bump metallizations have been investigated. With the help of the scanning electron microscopy and transmission electron microscopy it was discovered that the first phase to form was the metastable nanocrystalline ternary NiSnP layer that provided the substrate for the subsequent formation of $(Cu,Ni)_6Sn_5$. During cooling or in the subsequent reflows the metastable NiSnP layer partially transformed into the columnar Ni_3P. In this transformation Sn atoms and impurities, which do not dissolve into the Ni_3P, diffuse towards the remaining NiSnP layer. When the specimens are further annealed in solid state at 170°C the Ni_3P phase transforms into Ni_5P_2 implying that some more Ni has diffused towards the solder. However, when Ni(P)/Au finishes with a higher P content were used, only the ternary NiSnP layer was observed. Based on the mass balance and available thermodynamic data on the Sn–P–Ni system the evolution of the observed microstructures in the reactions between the solder and Ni(P)/Au finishes is discussed.

Reference

1. B. Salam, N. N. Ekere, and D. Rajkumar, "Study of the interface microstructure of Sn–Ag–Cu lead–free solders and the effect of solder volume on intermetallic layer formation", *51st Electronic Components and Technology Conference*, 29 May–1 June, 2001, pp.471–477.
2. Digital Object Identifier 10.1109/ECTC.2001.927769 Directive 2002/96/EC of the European Parliament and of the council on Waste of Electrical and Electronic Equipment (WEEE), Jan. 27th, 2003.
3. Directive 2002/95/EC of the European Parliament and of the council on the Restriction of the use of Hazardous Substances in Electronic and Electronic Equipment (RoHS), Jan. 27th, 2003.

4. Commission decision 2005/618/EC amending directive 2002/95/EC of the European Parliament and of the Council for the purpose of establishing the maximum concentration values for certain hazardous substances in electrical and electronic equipment, Aug. 18th, 2005.
5. K. N. Tu, A. M. Gusak, and M. Li, "Physical and materials challenges for lead–free solders", *Journal of Applied Physics*, **93**, 3, (2003), pp.1335–1353.
6. W. Peng, K. Zeng, and J. Kivilahti, "A literature review on potential lead–free solder systems", Espoo, Helsinki University of Technology, Report Series HUT–EPT–1, (2000), p. 53.
7. P. T. Vianco and D. R. Frear, "Issues in the replacement of lead–bearing solders", *Journal of Metals*, **45,** 7, (1993), pp. 14–19.
8. C. M. Miller, I. E. Anderson, and J. F. Smith, "A viable tin–lead solder substitute: Sn–Ag–Cu", *Journal of Electronic Materials*, **23**, 7, (1994), pp. 595–601.
9. I. E. Anderson, "Tin–silver–copper: a lead free solder for broad applications", *The Proceedings of the NEPCON West'96*, Anaheim, CA, March 25–28, 1996, IEEE, **2**, (1996), pp. 882–885.
10. E. Bradley and J. Hranisavljevic, "Characterization of the melting and wetting of Sn–Ag–X solders", *IEEE Transactions on Electronics Packaging Manufacturing*, **24**, 4, (2001), pp. 255–260.
11. "D5.1 Analysis of the current status of European lead–free soldering 2004", Germany, European Lead–Free Soldering Network, NMP2–CT–2003–505504, (2005), p. 22.
12. "NEMI group recommends tin/silver/copper alloy as industry standard for lead–free solder reflow in board assemblies", Press release on Jan. 24, 2000, http://www.inemi.org/cms/newsroom/PR/2000/PR012400.html, (14.7.2005).
13. J. K. Kivilahti, "The chemical modeling of electronic materials and interconnections ", *Journal of Metals*, **54**, 12, (2002), pp. 52–57(6).
14. C. F. Coombs Jr., *Printed Circuits Handbook*, 5th ed., New York, 2001, McGraw–Hill, p. 1200.
15. Y. S. Touloukian and C. Y. Ho, *Thermal Expansion: Metallic Elements and Alloys*, New York, 1975, IFI/Plenum, p. 316.
16. J. H. Hau and D. W. Rice, "Solder joint fatigue in surface mount technology: state of the art ", *Solid State Technology*, **28**, 10, (1985), pp. 91-104.

17. Sohn, J. E. "Are lead-free solder joints reliable", *Circuits Assembly*, June (2002), pp. 32–35.
18. T. Hirano, K. Fukuda, K. Ito, T. Kiga, and Y. Taniguchi, "Reliability of lead free solder joint by using chip size package". *Proceedings of the 2001 IEEE International Symposium on Electronics and the Environment, 2001.*, Denver, CO, May 7–9, 2001, pp.285–289.
19. A. Syed, "Reliability and Au embrittlement of lead free solders for BGA applications", *Proceedings. International Symposium on Advanced Packaging Materials: Processes, Properties and Interfaces, 2001*, Braselton, GA, Mar. 11–14, 2001, pp. 143–147.
20. S. R. Lee, B. H. W. Lui, Y. H. Kong, B. Baylon, T. Leung, P. Umali, and H. Agtarap, "Assessment of board level solder joint reliability for PBGA assemblies with lead-free solder joint", *Soldering & Surface Mount Technology*, **14**, 3, (2002), pp. 46–50(5)
21. E. Bradley and K. Banerji, "Effect of PCB Finish on the Reliability and Wettability of Ball Grid Array Packages", *IEEE Transactions on Components, Packaging, and Manufacturing Technology, Part B: Advanced Packaging*, **19**, 2, May (1996), pp. 320–330
22. T. T. Mattila, V. Vuorinen, and J. K. Kivilahti, "Impact of printed wiring board coatings on the reliability of lead–free chip–scale package interconnections", *Journal of Materials Research*, **19**, 11, (2004), pp. 3214–3223.
23. J.Koivisto, "Lyijyttömän juoteliitoksen mikrorakenne", master's thesis, Helsinki University of Technology, (2004), p. 73.
24. J. Karppinen, "Tehosyklaus- ja lämpöshokkitestauksen vaikutukset lyijyllisiin sekä lyijyttömiin komponenttiliitoksiin", master's thesis, Helsinki University of Technology, (2006), p. 125.
25. S. J. Ham, M. S. Chao and S. B. Lee, "Thermal deformations of CSP assembly during temperature cycling and power cycling", *International Symposium on Electronic Materials and Packaging, 2000. (EMAP 2000)*, Hong Kong, Nov.30–Dec.2, 2000, pp. 350–357.
26. D. E. H. Popps, A. Mawer, and G. Presas, "Flip chip PBGA solder joint reliability: power cycling versus thermal cycling", *IMAPS Topical Workshop and Exhibition on Flip Chip Technology*, Austin, TX, Jun. 15–18, 2003.

27. T. H. Wang, C.-C. Lee, Y.-S. Lai, and C.-E. Huang, "Correlation between power cycling and thermal cycling fatigue reliabilities of chip-scale packages", *IEEE/CPMT/SEMI 29th International Electronics Manufacturing Technology Symposium, 2004*, Jul.14–16, 2004, pp. 26-30.
28. S. K. W. Seah, C. T. Lim, E. H. Wong, V. B. C. Tan, and V. P. W. Shim, "Mechanical response of PCBs in portable electronic products during drop impact", *4th Electronics Packaging Technology Conference,* Singapore, Dec.10–12, 2002, pp.120 – 125.
29. C. T. Lim, and Y. J. Low, "Investigating the drop impact of portable electronic products", *the Proceedings of the 52nd Electronic Components and Technology Conference,* (2002), pp.1270 – 1274.
30. C. T. Lim, Y. M. Teo, V. P. W. Shim, "Numerical simulation of the drop impact response of a portable electronic product", *IEEE Transactions on Components, Packaging and Manufacturing Technology, Part A: Packaging Technologies*, **25**, 3, (2002) pp.478 – 485.
31. JESD22–B111, "Board level drop test method of components for handheld electronic products", JEDEC Solid State Technology Association, 2003, p. 16.
32. IEC 91/530/NP, "Surface mounting technology – Environmental and endurance test methods for surface mount solder joint. Part 3: cyclic drop test", International Electrotechnical Commission, proposal (26.9.2005), p. 14.
33. T. T. Mattila and J. K. Kivilahti, "Failure mechanisms of lead–free chip scale package interconnections under fast mechanical loading", *Journal of Electronic Materials*, **34**, 7, (2005), pp. 969–976.
34. T. O. Reinikainen, P. Marjamäki, and J. K. Kivilahti, "Deformation Characteristics and Microstructural Evolution of SnAgCu Solder Joints", *Proceedings of the 6th International Conference on Thermal, Mechanical and Multi-Physics Simulation and Experiments in Micro-Electronics and Micro-Systems, 2005. EuroSimE 2005*, Berlin, Apr.18–20, 2005, pp. 91–98.
35. T. T. Mattila, P. Marjamäki, and J. K. Kivilahti, "Reliability of CSP interconnections under mechanical shock loading conditions", *IEEE Transactions on Components and Packaging Technologies*, (in print).
36. T.Laurila, V.Vuorinen and J.K.Kivilahti, "Interfacial reactions between lead-free solders and common base materials", *Materials Science and Engineering - A Review Journal*, **49**, Nos 1-2, (2005), pp. 1–60.

37. C.E. Ho, R. Y. Tsai, Y. L. Lin and C. R. Kao, "Effect of Cu concentration on the reaction on between Sn-Ag-Cu solders and Ni", *Journal of Electronic Materials*, **31**, 6, (2002), pp. 584–590.
38. Chih-Hao Lin, Sinn-Wen Chen, and Chao-Hong Wang, "Phase Equilibrium and Solidification Properties of Sn-Cu-Ni alloys", *Journal of Electronic Materials*, **31**, 9, (2002), pp. 907–915.
39. S.-W. Chen, S.-H. Wu and S.-W Lee, "Interfacial Reactions in the Sn-(Cu)/Ni, Sn-(Ni)/Cu and Sn/(Cu,Ni) Systems", *Journal of Electronic Materials*, **32**, 11, (2003), pp. 1188–1194.
40. V. Vuorinen, H.Yu, and J.K.Kivilahti, "Formation of the intermetallic compounds between liquid Sn and different CuNix metallizations", in preparation.
41. M. Kulojärvi, "Reliability characterisation of lead-free and mixed technology FBGA assemblies", master's thesis, Helsinki University of Technology, (2001), p. 106.
42. Z. Mei, M. Kaufmann, A. Eslambolchi, and P. Johnson, "Brittle Interfacial Fracture of PBGA Packages Soldered on Electroless Nickel / Immersion Gold", *Proceeding of 48th Electronic Components and Technology Conference*, Seattle, WA, May 25–28, 1998, pp. 952 – 961.
43. Z. Mei, P. Johnson, M. Kaufmann, and A. Eslambolchi, "Effect of electroless ni / immersion au plating parameters on PBGA solder joint attachment reliability", *Proceeding of 49th Electronic Components and Technology Conference*, San Diego, CA, Jun. 1–4, 1999, pp. 125–134.
44. R. J. James, "Effect of temperature on mechanical shock reliability of high density WL-CSP intercneections", master's thesis, Helsinki University of Technology, (2006) , p.78.
45. T. T. Mattila and J. K. Kivilahti, "Reliability of lead–free interconnections under consecutive thermal and mechanical loadings", *Journal of Electronic Materials*, **35**, 2, (2006), pp.250-256(7).
46. L. Xu, J. H. L. Pang, K. H. Prakash, and T. H. Low, "Isothermal and thermal cycling aging on IMC growth rate in lead-free and lead-based solder interface", *IEEE Transactions on Components and Packaging Technologies*, **28**, 3, (2005), pp. 408-414.

47. K. N. Tu, "Cu/Sn interdiffusion reactions: thin film case vs. bulk case", *Materials Chemistry and Physics*, **46**, 2, Nov. (1996), pp. 217-223(7).
48. Z. Mei, A. Sunwoo, and J. Morris, "Analysis of low-temperature intermetallic growth in Copper-Tin diffusion couples", *Metallurgical Transaction A (USA)*, **23A**, 3, (1992), pp. 857-864.
49. M. Oh, "Growth kinetics and intermetallic phases in the Cu-Sn binary and the Cu-Ni-Sn ternary systems at low temperatures", doctoral dissertation, Lehigh University, (1994), p. 161.
50. K. J. Rönkä, F. J. J. Van Loo, and J. K. Kivilahti, "A Diffusion-Kinetic Model for Predicting Solder/Conductor Interactions in High Density Interconnection", *Metallurgical and Materials Transactions A*, **29A**, (1998), pp. 2951-2956.
51. A. Paul, "The kirkendall effect in solid state diffusion", doctoral dissertation, Technical University of Eindhoven, (2004), p.165.
52. K. Zeng, R. Stierman, T.-C. Chiu, D. Edwards, K. Ano, and K. N. Tu, "Kirkendall void formation in eutectic SnPb solder joints on bare Cu and its effect on joint reliability", *Journal of Applied Physics*, **97**, 024508 (2005), pp. 024508-1 – 024508-8.
53. Z. Mei, M. Ahmad, M. Hu, and G. Ramakrishna, "Kirkendall voids at Cu/solder interface and their effects on solder joint reliability", *Proceeding of the 55th Electronic Components and Technology Conference*, Lake Buena Vista; FL, May 31–Jun.3, 2005, pp. 415– 420.
54. Ning-Cheng Lee, "Optimizing the reflow profile via defect mechanism analysis", *Soldering & Surface Mount Technology*, **11**, 1, (1999), pp. 13–20.
55. F. Sarvar and P.P. Conway, "Effective transient process modeling of the reflow soldering of printed circuit assemblies", *Inter-Society Conference on Thermal Phenomena in Electronic Systems, 1996. I-THERM V.*, Orlando, FL, May 29–Jun 1, 1996, pp.195–202.
56. P.P. Conway, D.C. Whalley, M. Wilkinson and D.J. Williams, "Automated adaptive control of the reflow soldering of electronic assemblies", *21st IEEE/CPMT International Electronics Manufacturing Technology Symposium*, Austin, TX, Oct. 13–15, 1997, pp. 229–236.
57. F. Sarvar and P.P. Conway, "Effective modeling of the reflow soldering process: basis, construction, and operation of a process model", *IEEE*

Transactions on Components, Packaging and Manufacturing Technology-Part C, **21**, 2, (1998), pp.126–133.

58. F. Sarvar and P.P. Conway, "Effective modeling of the reflow soldering process: use of a modeling tool for product and process design", *IEEE Transactions on Components, Packaging and Manufacturing Technology-Part C*, **21**, 3, (1998), pp.165–171.
59. D.C.Whalley, and S.M.Hyslop, "A simplified model of the reflow soldering process", *Soldering & Surface Mount Technology*, **14**, 1, (2002), pp. 30–37(8).
60. M.A. Eftychiou, T.L. Bergman, and G.Y. Masada, "Thermal effects during infrared solder reflow – part II. A model of the reflow process", *ASME J. Electronic Packaging*, **114**, (1992), pp.48–54.
61. M.A. Eftychiou, T.L. Bergman, and G.Y. Masada, "A Detailed Thermal Model of the Infrared Reflow Soldering Process", *ASME J. Electronic Packaging*, **115**, (1993), pp.55–62.
62. M.D. Kannapel and A.J. Przekwas, "CFD model of the reflow soldering process and equipment". Report of CFD Research Corporation, M.R., (1997).
63. Kim, I.A.E. Daewoo, Y.K. Choi, G.B. Lee, I.Y. Chung and J.D. Kim, "Thermal investigation of an infrared reflow furnace with a convection fan", *Inter-Society Conference on Thermal Phenomena in Electronic Systems, 1996. I-THERM V.*, Orlando, FL, May 29–Jun 1, 1996, pp.211–216.
64. R. Niebling, R. Stehling, M. Nowottnick and K. Wittke, "Combined IR and forced Convection in Reflow Soldering", *Surface Mount Technology Magazine*, **12**, 8, (1998), pp. 138–140.
65. D.A.Anderson, J.C.Tannehill, and R.H.Pletcher, *Computational fluid mechanics and heat transfer*, New York, 1984, McGraw-Hill Book Co., p. 609.
66. C.Hirsch, *Numerical Computation of Internal and External Flows Volume 2, Computational Methods for Inviscid and Viscous Flows*, John Wiley & Sons Ltd., 1990, p.714.
67. C.A.J.Fletcher, *Computational Techniques for Fluid Dynamics*, New York, 1997, Springer-Verlag Berlin and Heidelberg GmbH & Co. K, p. 364.
68. J.H.Ferziger and M.Peric, *Computational Methods for Fluid Dynamics*, New York, 1996, Springer-Verlag Berlin and Heidelberg GmbH & Co. K, p. 370.

69. F.P.Incropera and D.P. DeWitt, *Fundamentals of Heat and Mass Transfer*, 3rd Edition, New York, 1990, John Wiley & Sons Ltd., p. 919.
70. T.Massalski, *Binary Alloy Phase Diagrams (ASM handbook)*, 10th edition, 1992, ASM International, p.512.
71. L. Kaufman and H. Bernstein, *Computer calculation of phase diagrams with special reference to refractory metals*, New York, 1970, Academic Press, p.334.
72. N. Saunders and A.P. Miodownik, *CALPHAD (Calculation of Phase Diagrams): A Comprehensive Guide (Pergamon Materials Series)*, 1998, Pergammon, p. 496.
73. M.Hillert, *Phase Equilibria, Phase Diagrams and Phase Transformations: Their Thermodynamic Basis*, Cambridge University Press, 1998, p.554.
74. J.K.Kivilahti, "The chemical modeling of electronic materials and interconnections", *Journal of Metals*, **54**, 12, (2002), pp. 52–57.
75. W.Peng, "Lead-free electronic assembly based on Sn-Ag-Cu solders", licentiate thesis, Helsinki University of Technology, (2001), p. 124.
76. M.E.Loomans and M.E.Fine, "Tin-Silver-Copper eutectic temperature and composition", *Metallurgical & Materials Transactions A.*, **31A**, 4, (2000), pp. 1155–1162,.
77. K.-W.Moon, W.J.Boettinger, U.R.Kattner, F.S.Biancaniello, A.A.Handwerker, "Experimental and thermodynamic assessment of Sn-Ag-Cu solder alloys", *Journal of Electronic Materials*, **29**, 10, (2000), pp. 1122–1136.
78. K. Zeng and K. N. Tu, "Six cases of reliability study of Pb-free solder joints in electron packaging technology," *Materials Science and Engineering Reports*, **R38**, 2, Jun. (2002), pp. 55–105.
79. L.Garner, S.Sane, D.Suh, T.Byrne, A.Dani, T.Martin, M.Mello, M.Patel, R.Williams, "Finding solutions to the challenges in package interconnect reliability", *Intel Technology Journal*, **9**, 4, (2005), pp. 297–308.
80. T.M.Korhonen and J.K.Kivilahti, "Thermodynamics of the Sn-In-Ag solder system", *Journal of Electronic Materials*, **27**, 3, (1998), pp. 149–158.
81. J.K.Kivilahti and P.Savolainen, "Anisotropic adhesives for flip-chip bonding", *Journal of Electronics Manufacturing*, **5**, 4, (1995), pp. 245–252.

82. J.S.Kirkaldy, "Diffusion in multicomponent metallic systems: I. phenomenological theory for substitutional solid solution alloys", *Canadian Journal of Physics*, **36**, (1958), 899–925,
83. F.J.J. van Loo, "Multiphase diffusion in binary and ternary solid-state systems", Prog. Solid State Chem., **20**, 1, (1990), pp. 47–99,
84. D.Turnbull, "Formation of Crystal Nuclei in Liquid Metals", *Journal of Applied Physics*, **21**, 10, (1950), pp.1022–1028.
85. B.Cantor and R.D.Doherty, "Heterogeneous Nucleation in Solidifying Alloys", Acta Metallurgica., **27**, 1, (1979), pp. 33–46.
86. F.J.J. van Loo, G.F.Bastin and J.W.G.A.Vrolijk, "A Practical Solution for the Diffusion Equations in Binary and Multicomponent Systems with Constant Intrinsic Diffusion Coefficients", Metallurgical Transaction, 18A, 801–809, (1987)
87. J.S.Kirkaldy and D.J.Young, *Diffusion in the Condensed State*, London, 1987, The Institute of Metals, p. 527.
88. K.N.Tu, "Irreversible processes of spontaneous whiesker growth in bimetallic Cu-Sn thin-film reactions", *Physical Review B*, **49**, 3, (1994) pp. 2030–2034.
89. K.N.Tu, "Electromigration in Stressed Thin Films", *Physical Review B*, **45**, 3, (1992), pp.1409-1413.
90. V.I.Dybkov, "Reaction Diffusion in Heterogeneous Binary Systems. Part 1: Growth of the Chemical Compound Layers at the Interface between Two Elementary Substances: One Compound Layer", *Journal of Materials Science*, **21**, 9, (1986), pp. 3078–3084,.
91. V.I.Dybkov, "Reaction Diffusion in Heterogeneous Binary Systems. Part 2: Growth of the Chemical Compound Layers at the Interface between Two Elementary Substances: Two Compound Layers", *Journal of Materials Science*, **21**, 9, (1986), pp. 3085-3090.
92. V.I.Dybkov, "Reaction Diffusion in Heterogeneous Binary Systems. Part 3: Multiphase Growth of the Chemical Compound Layers at the Interface between Two Mutually Insoluble Substances", *Journal of Materials Science*, **22**, 12, (1986), pp. 4233-4239.